Tuning of the Chl_$D1$ and Chl_$D2$ properties in photosystem II by site-directed mutagenesis of neighbouring amino acids

Miwa Sugiura, Masaya Kimura, Naohiro Shimamoto, Yuki Takegawa, Makoto Nakamura, Kazumi Koyama, Julien Sellés, Alain Boussac, A. William Rutherford

BBA - Bioenergetics 1865 (2024) 149013

Contents lists available at ScienceDirect

BBA - Bioenergetics

journal homepage: www.elsevier.com/locate/bbabio

Tuning of the Chl_{D1} and Chl_{D2} properties in photosystem II by site-directed mutagenesis of neighbouring amino acids

Miwa Sugiura [a,*], Masaya Kimura [a], Naohiro Shimamoto [a], Yuki Takegawa [a], Makoto Nakamura [a], Kazumi Koyama [a], Julien Sellés [b], Alain Boussac [c,*], A. William Rutherford [d]

[a] Proteo-Science Research Center, Department of Chemistry, Graduate School of Science and Technology, Ehime University, Bunkyo-cho, Matsuyama, Ehime 790-8577, Japan
[b] Institut de Biologie Physico-Chimique, UMR CNRS 7141 and Sorbonne Université, 13 rue Pierre et Marie Curie, 75005 Paris, France
[c] Institut de Biologie Intégrative de la Cellule, UMR9198, CEA Saclay, 91191 Gif-Sur-Yvette, France
[d] Department of Life Sciences, Imperial College, SW7 2AZ London, UK

ARTICLE INFO

Keywords:
Photosystem II
Reaction center
Chl_{D1}
Chl_{D2}
P_{680}
Photoinhibition
Electrochromic band-shift

ABSTRACT

Photosystem II is the water/plastoquinone photo-oxidoreductase of photosynthesis. The photochemistry and catalysis occur in a quasi-symmetrical heterodimer, D1D2, that evolved from a homodimeric ancestor. Here, we studied site-directed mutants in PSII from the thermophilic cyanobacterium *Thermosynechoccocus elongatus*, focusing on the primary electron donor chlorophyll *a* in D1, Chl_{D1}, and on its symmetrical counterpart in D2, Chl_{D2}, which does not play a direct photochemical role. The main conserved amino acid specific to Chl_{D1} is D1/T179, which H-bonds the water ligand to its Mg^{2+}, while its counterpart near Chl_{D2} is the non-H-bonding D2/I178. The symmetrical-swapped mutants, D1/T179I and D2/I178T, and a second Chl_{D2} mutant, D2/I178H, were studied. The D1 mutations affected the 686 nm absorption attributed to Chl_{D1}, while the D2 mutations affected a 663 nm feature, tentatively attributed to Chl_{D2}. The mutations had little effect on enzyme activity and forward electron transfer, reflecting the robustness of the overall enzyme function. In contrast, the mutations significantly affected photodamage and protective mechanisms, reflecting the importance of redox tuning in these processes. In D1/T179I, the radical pair recombination triplet on Chl_{D1} was shared onto a pheophytin, presumably Phe_{D1} and the detection of $^3Phe_{D1}$ supports the proposed mechanism for the anomalously short lifetime of $^3Chl_{D1}$; *e.g.* electron transfer quenching by Q_A^- of $^3Phe_{D1}$ after triplet transfer from $^3Chl_{D1}$. In D2/I178T, a charge separation could occur between Chl_{D2} and Phe_{D2}, a reaction that is thought to occur in ancestral precursors of PSII. These mutants help understand the evolution of asymmetry in PSII.

1. Introduction

Oxygenic photosynthesis in cyanobacteria, algae and higher plants converts solar energy into the chemical bonds of biological carbon polymers and of dioxygen. Photosystem II (PSII) begins this process by splitting water to obtain electrons in the form of reduced quinone, while generating a proton gradient and releasing O_2. In cyanobacteria, the PSII complex comprises 17 trans-membrane subunits. These subunits bind 35 chlorophylls (Chl), 2 pheophytins (Phe), a b-type cytochrome ($Cytb_{559}$), 1 non-heme iron, 2 plastoquinones (Q_A and Q_B), the Mn_4CaO_5 cluster, 2 Cl^-, 12 carotenoids and 25 lipids [1,2]. In cyanobacteria, PSII binds 3 extrinsic membrane subunits, PsbO, PsbU and the c-type $Cytc_{550}$ (PsbV) [1,2].

Solar energy conversion into chemical energy starts with the

Abbreviations: Chl, chlorophyll; Chl_{D1}/Chl_{D2}, monomeric Chl on the D1 or D2 side, respectively; Cyt, cytochrome; DCMU, 3-(3,4-dichlorophenyl)-1,1-dimethylurea; DMPO, 5,5-dimethyl-1-pyrroline-N-oxide; DMSO, dimethyl sulfoxide; EPR, Electron Paramagnetic Resonance; MES, 2-(*N*-morpholino) ethanesulfonic acid; P_{680}, primary electron donor; P_{D1} and P_{D2}, individual Chl on the D1 or D2 side, respectively, which constitute a pair of Chl with partially overlapping aromatic rings; Phe_{D1} and Phe_{D2}, pheophytin on the D1 or D2 side, respectively; PPBQ, phenyl *p*–benzoquinone; PSII, Photosystem II; Q_A, primary quinone acceptor; Q_B, secondary quinone acceptor; TL, thermoluminescence; Tyr_D, the tyrosine 160 of D2 acting as a side-path electron donor of PSII; Tyr_Z, the tyrosine 161 of D1 acting as the electron donor to P_{680}; WT*3, *T. elongatus* mutant strain deleted *psbA*$_1$ and *psbA*$_2$ genes and with a His-tag on the carboxy terminus of CP43; WT', *T. elongatus* mutant strain deleted *psbA*$_1$, *psbA*$_2$ and *psbD*$_2$ genes and with a His-tag on the carboxy terminus of CP43.

* Corresponding authors.
E-mail addresses: miwa.sugiura@ehime-u.ac.jp (M. Sugiura), alain.boussac@cea.fr (A. Boussac).

https://doi.org/10.1016/j.bbabio.2023.149013
Received 11 July 2023; Received in revised form 1 September 2023; Accepted 11 September 2023
Available online 17 September 2023

absorption of a photon by a Chl forming an excited state. Most chlorophylls play light-collecting roles and when one is excited, the excitation energy is then transferred to other chlorophylls until it reaches the key pigments in photochemical reaction centre [3]: 4 Chl-*a* molecules, P_{D1}, P_{D2}, Chl_{D1}, Chl_{D2} and 2 Phe-*a* molecules, Phe_{D1} and Phe_{D2} (Fig. 1A) [4–8]. Most of the Chl bound to PSII have histidine ligands to their Mg^{2+} ions, including P_{D1} and P_{D2} with the D1/H198 and D2/H197, respectively, (Fig. 1A) [1,2]. In contrast, Chl_{D1} has a water ligand that is hydrogen bonded to D1/T179, while the water ligand to Chl_{D2} is not involved in H-bonding since the D2/I178 residue, corresponding to D1/T179, is unable to accept an H-bond (Fig. 1B).

There is a consensus that Chl_{D1} is the lowest site energy, *e.g.* [9,10], and the primary donor [5,9,11]. At room temperature, although the excited state is more distributed on the core pigments and onto the antenna, Chl_{D1} remains the longest wavelength species and thus $^*Chl_{D1}$ is the most populated excited state. It has been reported that two kinetically distinct steps are observed in the charge separation process at 77 K: a fast one occurring in the ~1 to 5 ps time-range, which is attributed to the $^*[Chl_{D1}Phe_{D1}] \rightarrow Chl_{D1}^{+}Phe_{D1}^{-}$ reaction; and a slower one occurring in 25–30 ps time-range attributed to the $^*[P_{D1}Chl_{D1}] \rightarrow P_{D1}^{+}Chl_{D1}^{-}$ reaction [6]. But some data, arguments and calculations suggest that Chl_{D1} is the only or dominant primary donor under physiological conditions [5,8,9,12].

In either mechanism, the first stabilisation step results in formation of the $[P_{D1}P_{D2}]^{+}Phe_{D1}^{-}$ radical pair, where the cation is mainly localised on P_{D1}, and the radical pair is further stabilised by the electron transfer from Phe_{D1}^{-} to Q_A, the primary quinone electron acceptor, and then to Q_B, the exchangeable quinone electron acceptor. While Q_A can only be singly reduced and functions as an unprotonated, one-electron relay under normal conditions, Q_B accepts two electrons and two protons before leaving its binding site and being replaced by an oxidized plastoquinone molecule from the membrane plastoquinone pool, *e.g.* [13–15]. On the oxidizing side of PSII, P_{D1}^{+} oxidizes Tyr_Z, the Tyr161 of the D1 polypeptide. The $Tyr_Z^{\bullet}$ radical is then reduced by the Mn_4CaO_5 cluster. After four charge separations, the Mn_4CaO_5 cluster accumulates four oxidizing equivalents and thus cycles through five redox states denoted S_0 to S_4. Upon formation of the S_4-state, two molecules of water are oxidized, the S_0-state is regenerated and O_2 is released [16,17] (and see *e.g.* [18,19] for reviews).

In O_2 evolving PSII, the electron transfer from Tyr_Z to P_{D1}^{+} takes place in time-ranges from tens of ns to tens of μs. According to the current understanding of the multiphasicity of the reduction of $[P_{D1}P_{D2}]^{+}$, the ns components are kinetically limited by the electron transfer process, whereas the μs phases are kinetically limited by proton-coupled reactions, *e.g.* [20]. The fastest electron transfer from Tyr_Z to P_{D1}^{+} occurs with a $t_{1/2}$ close to 20 ns [21,22]. The μs to tens-of-μs phases correspond to proton movements in which the phenolic proton of the $Tyr_Z^{\bullet}$ radical moves, in a first step, onto the H-bonded D1/His190 [23].

The evolution of PSII photochemistry, including the role of Chl_{D1} and Chl_{D2} in charge separation and comparisons with the purple bacterial reaction centre, has been discussed elsewhere [3,24,25]. It seems clear that the pseudo-symmetrical structure of PSII, with D1/D2 as the site of the photochemistry and both catalytic sites, (namely: *i*) quinone reduction, and *ii*) water oxidation), has evolved from a homodimeric ancestor in which charge separation and, most likely, catalysis, took place symmetrically on both sides of the homodimeric D/D proto-PSII [4]. The specialized asymmetric D1/D2 PSII evolved for efficiency and survival with charge separation now taking place only one side of the D1/D2 dimer [4,25]. Chl_{D1} and Chl_{D2} are symmetrically arranged and their ancestral counterparts may have both functioned as primary donors in the homodimeric ancestor. The main difference in the environment of Chl_{D1} that distinguishes it from Chl_{D2}, is the presence of a conserved threonine 179 in D1, which H-bonds the water molecule that is the axial ligand to the Mg^{2+} ion in Chl_{D1}. On the D2 side, the equivalent amino acid is a non-H-bonding isoleucine (D2/I178), which is also conserved. It seems likely that this threonine/isoleucine swap plays a

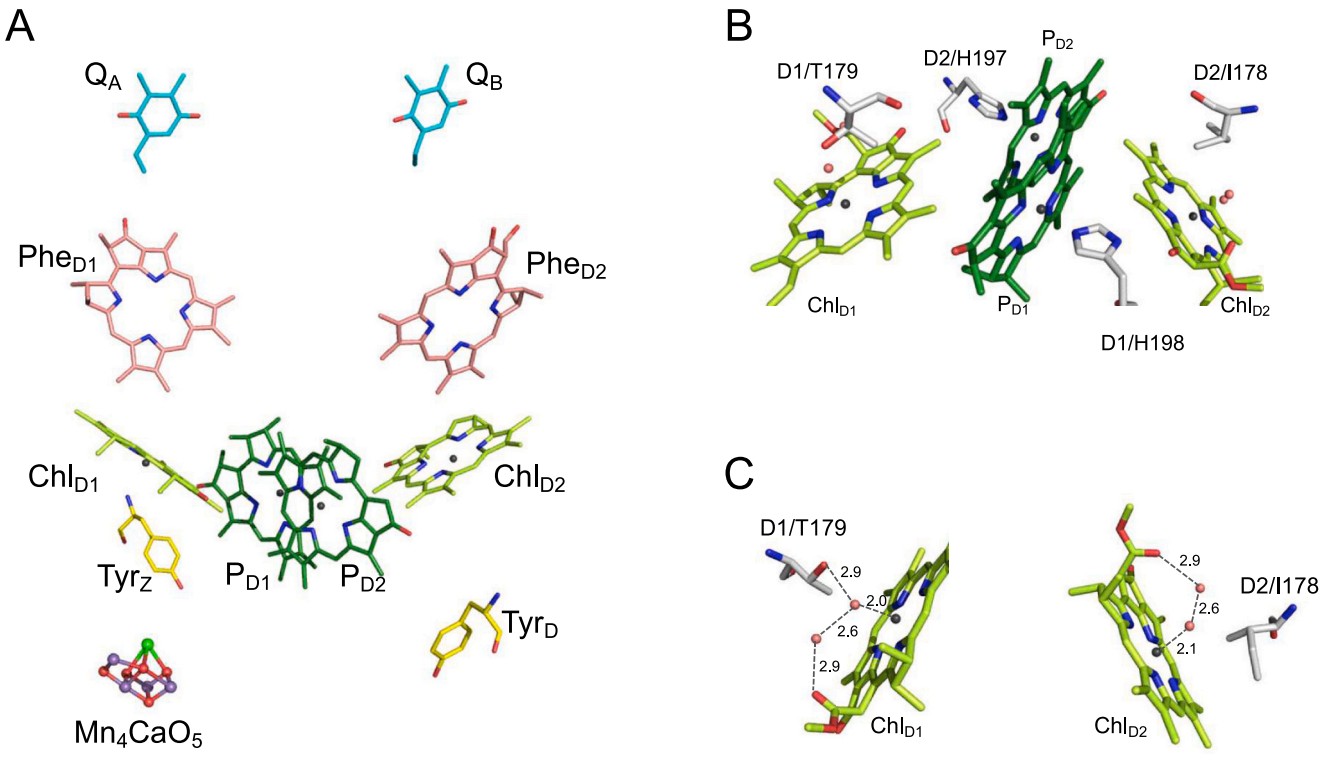

Fig. 1. Arrangement of cofactors in PSII reaction centre (A), structure of Chl_{D1}, P_{D1}, P_{D2}, and Chl_{D2} with amino acid ligands (B), and structure of the ligands of Chl_{D1} and Chl_{D2} (C). The figures were drawn in MacPyMOL with the A monomer in PDB 4UB6.

role in the asymmetry associated with the evolution of one-sided charge separation in PSII.

Experimentally, the Q_Y of Chl_{D1} was identified by the site-directed mutagenesis D1/T179H in *Synechocystis* 6803 [10] and more recently in PSII from *T. elongatus* [26]. The electrochromic band-shift of Chl_{D1} was centred ~681 nm in the wild type and was identified because it red-shifted by 2–3 nm in the D1/T179H mutant and blue-shifted by 1 nm in a D1/T179Q mutant [10]. This was the case *i*) when the bandshift was induced largely by P_{D1}^{+}, which dominated the effect when $P_{D1}^{+}Q_A^{-}$ was present in the ms timescale at 80 K, and *ii*) when Q_A^{-} was the main state responsible for the electrochromic shift in illumination-*minus*-dark spectra at 80 K [10]. Similar Q_A^{-}-induced band-shifts were obtained at ~77 K in *T. elongatus* in the D1/T179H PSII mutant [26].

The spectroscopic characterization of these mutants also confirmed that the triplet state, produced upon charge recombination from $^{3}[P_{680}^{+}Phe^{-}]$, was localised on Chl_{D1} [10,27], in agreement with earlier EPR [11] and infrared spectroscopy [28] studies.

The D1/T179H and D1/T179V mutants in *T. elongatus* were fully active for O_2 evolution and this allowed the thermoluminescence emission of these mutants to be studied [26]. The radiative $S_2Q_A^{-}$/DCMU recombination was interpreted as occurring *via* the repopulation of $^{*}Chl_{D1}$ itself and that the immediate precursor state of the radiative excited state was the $Chl_{D1}^{+}Phe_{D1}^{-}$ radical pair [26], as suggested in [24]. In addition, chlorophyll bleaching due to high intensity illumination correlated with the amount of $^{1}O_2$ generated. Comparison of the bleaching spectra with the Q_A^{-}-induced electrochromic shifts of the Chl_{D1} absorption spectrum, indicated that in the D1/T179H mutant and in the WT*3 PSII, the Chl_{D1} itself was the chlorophyll that was first damaged by $^{1}O_2$, whereas in the D1/T179V mutant, a longer wavelength, antenna chlorophyll was damaged. Thus, Chl_{D1} appears to be one of the primary sites of damage in recombination-mediated photoinhibition [26].

In this paper, we describe experiments aimed at characterizing new site-directed mutants modifying the environment of Chl_{D1} and Chl_{D2}. A range of biophysical methods (EPR, absorption spectroscopy at ~77 K, time-resolved UV–vis absorption spectroscopy, O_2 polarography, and thermoluminescence) and biochemical approaches (SDS-PAGE and immunoblot anti-DMPO antibody staining) were used to monitor the effects of the mutations on PSII activity, electron transfer, back-reactions and photodamage.

The mutants studied were constructed in a strain with PsbA3 as the

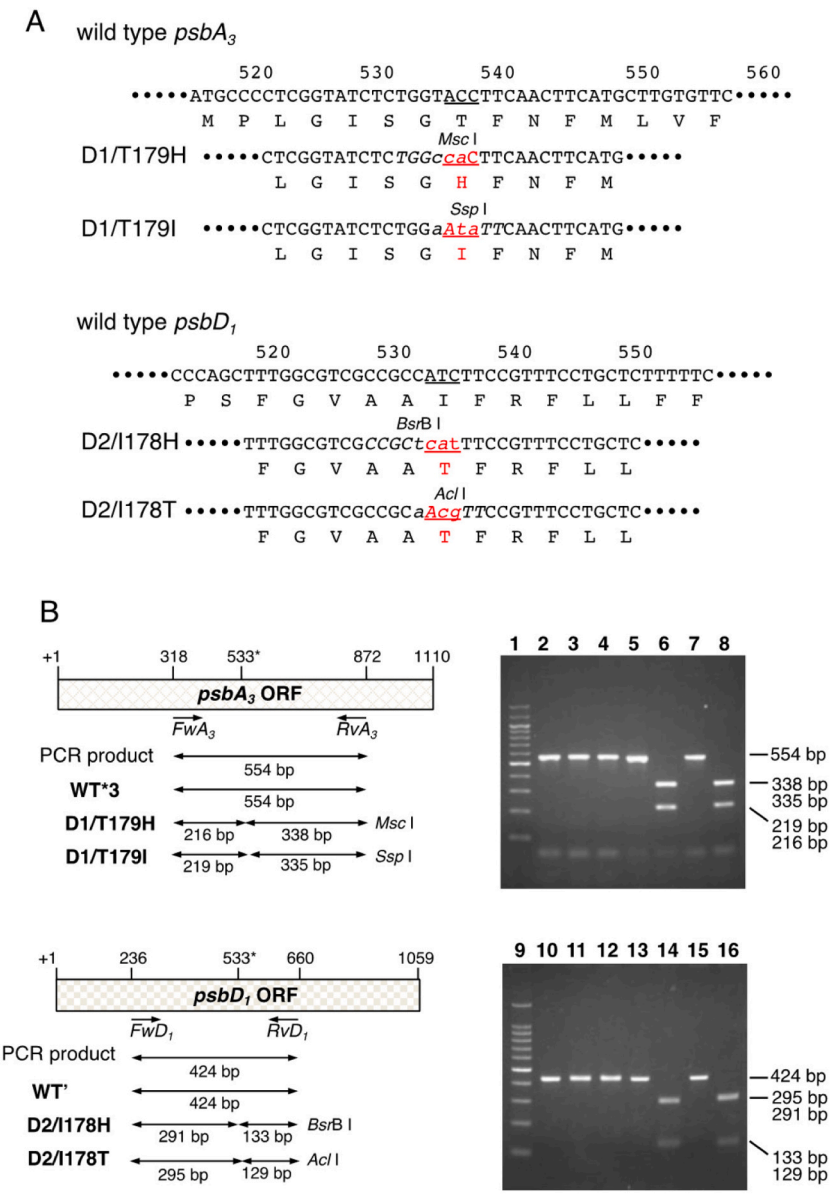

Fig. 2. Construction of the *psbA*$_3$ and *psbD*$_1$ genes in the D1/T179 and D2/I178 site-directed mutants, respectively. (A) Nucleotide sequences of *psbA*$_3$ and *psbD*$_1$ and their amino acid sequences around D1/T179 and D2/I178. Red letters indicate substituted amino acids. The text in italic shows the restriction site for creating the mutation. (B) Physical map around *psbA*$_3$ and *psbD*$_1$, and results of agarose gel electrophoresis. Asterisks are positions around mutation. PCR products using the primers were loaded on 2 % agarose gel before (lanes 2, 5, 7, 10, 13, and 15) and after digestion with restriction enzymes (lanes 3, 4, 6, 8, 11, 12, 14 and 16). Lanes 1 and 9, 100 bp DNA ladder markers (Nacalai, Japan); lanes 2 to 4, WT*3 strain; lanes 5 and 6, D1/T179H strain; lanes 7 and 8, D1/T179I strain; lanes 10 to 12,WT' strain; lanes 13 and 14, D2/I178H strain; lanes 15 and 16, D2/I178T strain. Amplified DNA were digested with *Msc* I (lanes 3 and 6), *Ssp* I (lanes 4 and 8), BsrB I (lanes 11 and 14), *Acl* I (lanes 12 and 16).

D1 protein and PsbD1 as the D2 protein. Four novel mutations were made and studied: *i*) the D1/T179I to make the environment of Chl_{D1} more like that of Chl_{D2}; *ii*) the D2/I178T to make the environment of Chl_{D2} more like that of Chl_{D1}; *iii*) the D2/I178H to make the environment of Chl_{D2} more like those of the majority of Chl-*a* molecules in PSII; and *iv*) the D1/T179H-D2/I178H, the symmetrical double histidine environment. For comparison, several experiments were also done in the D1/T179H previously studied [26].

2. Materials and methods

2.1. Construction of site-directed mutants

For the construction of the Chl_{D1} mutants, D1/T179H and D1/T179I, the *T. elongatus* strain used was the *ΔpsbA$_1$, ΔpsbA$_2$* deletion mutant [29], called WT*3, constructed from the *T. elongatus* 43-H strain that had a His_6-tag on the carboxy terminus of CP43 [30]. The construction of the D1/T179H site-directed mutant has been described earlier [26]. The D1/T179I mutant was constructed with the procedure described in [26]. As host cells for the Chl_{D2} mutants, D2/I179H and D2/I179T, the WT' strain (with deleted *psbA$_1$, psbA$_2$* and *psbD$_2$* genes and with a His-tag on the carboxy terminus of CP43 [29]) was used. Fig. 2 shows a summary of the constructions and confirmation of the site-directed mutations.

2.2. PSII samples

Fully active His-tagged PSII from the *T. elongatus* mutants were purified as previously described [31]. For the triplet EPR signal detection in Mn-depleted PSII, the samples were prepared as follows. For Mn-depletion, ~10 mM NH_2OH, from a stock at 1 M at pH 6.5, and 1 mM EDTA were added to the PSII samples. Then, the hydroxylamine was removed by washing of the PSII samples by cycles of dilution in 1 M betaine, 15 mM $CaCl_2$, 15 mM $MgCl_2$, 40 mM MES, 100 μM EDTA, pH 6.5, followed by concentration using Amicon Ultra-15 centrifugal filter units (cut-off 100 kDa), until the estimated residual NH_2OH concentration was lower than 0.1 μM in the concentrated PSII samples before the final dilution. In the final dilution step, the PSII samples were suspended in 1 M betaine, 15 mM $CaCl_2$, 15 mM $MgCl_2$, 100 mM MES, pH 6.5.

2.3. SDS-polyacrylamide gel electrophoresis of PSII polypeptides by high-light illumination

Purified PSII samples suspended in 40 mM MES/NaOH (pH 6.5) buffer containing 10 mM NaCl, 10 mM $CaCl_2$, 10 mM $MgCl_2$ and 0.03 % *n*-dodecyl-β-D-maltoside were illuminated at ~800 μmol photons m^{-2} s^{-1} for 20 min. The PSII (8 μg Chl each) before and after high-light illumination were solubilized with 2 % lithium laurylsulfate, and then loaded on an SDS-15 % polyacrylamide gel containing 7.5 M urea as previously described in [32]. The polypeptides were visualised by Coomassie brilliant blue R-250.

2.4. Immunoblot staining of protein radicals

Detection of radical proteins was done according to [33]. One μg Chl mL^{-1} of PSII complexes were mixed with 50 mM 5,5-dimethyl-1-pyrroline-N-oxide (DMPO) (Dojindo) as a spin trap, then the samples were illuminated at 800 μmol photons m^{-2} s^{-1} for 30 min. The high-light illuminated samples were loaded onto an SDS-15 % polyacrylamide gel containing 7.5 M urea (1 μg Chl each lane). After the electrophoresis, polypeptides on the gel transferred onto a polyvinylidene difluoride membrane (Hybond-P, GE Healthcare) by using a semi-dry electroblotter (Bio-Rad Laboratories). Polyclonal anti-DMPO antibody (Abcam) was used to detect radical proteins on the blots. The blots were developed with a goat anti-rabbit IgG-alkaline phosphatase conjugate (Santa Cruz Biotechnology).

2.5. Singlet oxygen production

Singlet oxygen production was detected by histidine-mediated oxygen uptake measurements under high-light illumination conditions (20,000 μmol photons m^{-1} s^{-1}) at 25 °C, as previously described in [26]. The activity was measured in 20 mM MES buffer (pH 6.5) containing 15 mM $CaCl_2$, 15 mM $MgCl_2$, 20 mM NaCl in the presence of 10 mM L-histidine and 25 μM 3-(3,4-dichlorophenyl)-1,1-dimethylurea (DCMU) at 2 μg Chl mL^{-1} by using a Clark-type oxygen electrode (Hansatech).

2.6. UV–visible time-resolved absorption change spectroscopy

Time-resolved absorption changes measurements were performed with a lab-built spectrophotometer [34] described in detail in [31]. For the ΔI/I measurements in O_2 evolving PSII the samples were diluted in 1 M betaine, 15 mM $CaCl_2$, 15 mM $MgCl_2$, and 40 mM MES (pH 6.5). PSII samples were then dark-adapted for ~1 h at room temperature (20–22 °C) before the addition of 0.1 mM phenyl *p*–benzoquinone (PPBQ) dissolved in dimethyl sulfoxide.

The chlorophyll concentration of all the samples was ~25 μg of Chl mL^{-1}. After the measurements, the ΔI/I values were normalized to exactly $A_{673} = 1.75$, that is very close to 25 μg Chl mL^{-1} with $\varepsilon \sim 70$ $mM^{-1}{\cdot}cm^{-1}$ at 674 nm for dimeric PSII [35].

2.7. High-light-minus-dark absorption spectra at room temperature

PSII complexes were suspended in 20 mM MES buffer (pH 6.5) containing 15 mM $CaCl_2$, 15 mM $MgCl_2$, 10 mM NaCl and 200 mM mannitol at 6.5 μg Chl mL^{-1}. Then, the PSII complexes were illuminated with ~500 μmol photons m^{-2} s^{-1} at 45 °C for 60 min. Absorption spectra of dark adapted PSII and high-light illuminated PSII were recorded using a spectrophotometer U-3900 (Hitachi High Tech. Co., Japan) at room temperature. The wavelength accuracy was ±0.2 nm, the spectral band-pass was 2 nm and the scan speed was 120 nm min^{-1}.

2.8. Light-induced absorption changes at 77 K

Light-induced absorption spectra were measured basically as in our previous paper [26] using a spectrophotometer U—3900H (Hitachi High Tech. Co., Japan) equipped with a cryostat OptistatCF (Oxford Instruments) for low temperature measurements. The PSII samples were suspended in 20 mM MES buffer (pH 6.5) containing 15 mM $CaCl_2$, 15 mM $MgCl_2$, 10 mM NaCl and 65 % glycerol. After dark adaption for 60 min, the PSII samples at 0.2 mg Chl mL^{-1} were illuminated for 30 s with a ~ 30 mW cm^{-2} cw light source (MSG3-1100S-SD; Moritex Co., Japan) to induce the formation of Q_A^- (the oxidized species in this experiment being mainly the $Cytb_{559}$ [26]). The wavelength accuracy was ±0.2 nm, the spectral band-pass was 2 nm and the scan speed was 120 nm min^{-1}.

2.9. EPR spectroscopy

X-band cw-EPR spectra were recorded with a Bruker Elexsys 500 X-band spectrometer equipped with a standard ER 4102 (Bruker) X-band resonator, a Bruker teslameter, an Oxford Instruments cryostat (ESR 900) and an Oxford ITC504 temperature controller. O_2-evolving PSII samples were loaded in the dark into quartz EPR tubes at 1.1 mg of Chl mL^{-1} and dark-adapted for 1 h at room temperature. The samples were then synchronized in the S_1-state with one pre-flash [36]. Flash illumination at room temperature was provided by a neodymium: yttrium–aluminum garnet (Nd:YAG) laser (532 nm, 550 mJ, 8 ns Spectra Physics GCR-230-10). After a further 1 h dark-adaptation at room temperature the samples were frozen in the dark to 198 K in a dry-ice/ethanol bath and then transferred into liquid N_2 (77 K). Prior to recording the spectra, the samples were degassed at 198 K. In these samples, the S_2 multiline state was induced by illumination with an 800 W tungsten lamp filtered by water and infrared cut-off filters for

approximately 5–10 s at 198 K in a non-silvered Dewar in ethanol cooled with dry ice.

For the recording of the triplet EPR signals, ~ 40 mM sodium dithionite (from a 1 M stock freshly prepared in water) was added into the EPR tube. The EPR tube were then illuminated for ~5 min at room temperature with the 800 W tungsten lamp described above to achieve the double reduction of Q_A in a high proportion of the centers [11]. Then, the samples were dark-adapted for ~30–60 min at room temperature to allow the Phe^- anion radical, also produced under the continuous illumination, to be reoxidized [11] prior to the freezing of the samples. The triplet EPR signals were then generated by continuous illumination at 4.2 K inside the EPR cavity [11]. The illumination was done with a low voltage halogen lamp (Philips GX5.3, 24 V, 250 W) filtered by water and infrared cut-off filters.

2.10. Thermoluminescence measurements

Thermoluminescence (TL) glow curves were measured with TL500 (Photon Systems Instruments). Ten μg of purified PSII were suspended in 50 μL of 40 mM MES buffer (pH 6.5) including 15 mM $MgCl_2$, 15 mM $CaCl_2$ and 1 M betaine. After dark-relaxation for 1 h on ice, 10 μM DCMU was added. 70 μL of the sample (10 μg Chl) was loaded onto 15 mm × 15 mm filter paper (0.23 mm thickness, Advantec No.3), then one saturating LED flash was given at −15 °C. The thermoluminescence emission was measured during warming the sample with a heating rate of 40 °C min^{-1}.

3. Results

3.1. Intactness of the purified mutant PSII's

All the *T. elongatus* mutant cells studied here were able to grow photo-autotrophically, although the growth of D2/I178T and D1/T179I cells were slower and more sensitive to light than other strains. The intactness of the purified PSII cores was monitored by the amplitude the period-of-four oscillations arising from absorption changes of the

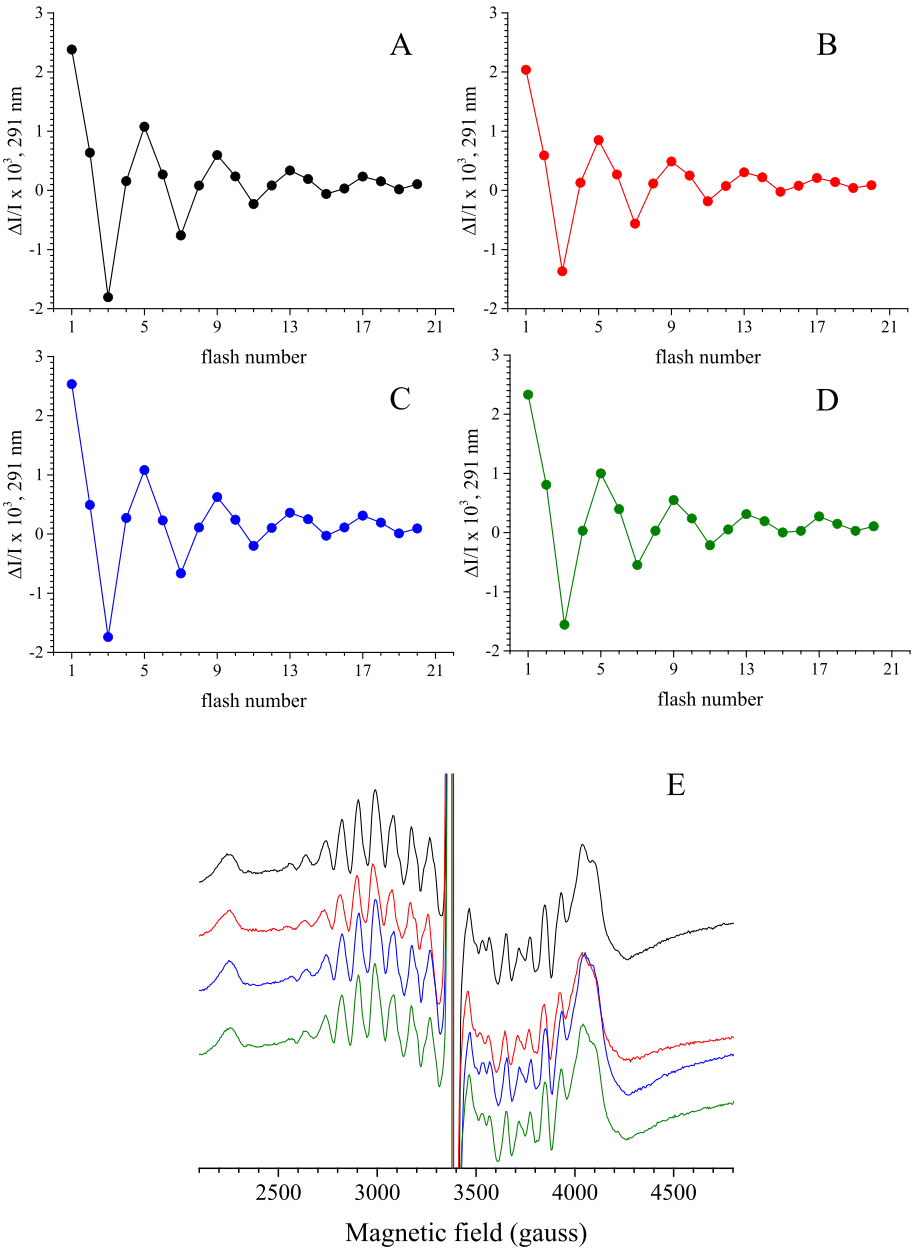

Fig. 3. Upper panels, sequence of the amplitude of the absorption changes at 291 nm using a series of saturating flashes spaced 400 ms apart. The measurements were done in PsbA3-PSII (black), D1/T179I-PSII (red), D2/I178T-PSII (blue), and D2/I178H-PSII (green). The samples ([Chl] = 25 μg mL^{-1}) were dark-adapted for 1 h at room temperature before the addition of the electron acceptor system, 100 μM PPBQ dissolved in dimethyl sulfoxide and 100 μM ferricyanide. The ΔI/I were measured 100 ms after each flash. The continuous lines joining the points are drawn for clarity. Lower Panel, EPR spectra recorded in PsbA3-PSII (black spectrum), D1/T179I-PSII (red spectrum), D2/I178T-PSII (blue spectrum) and D2/I178H-PSII (green spectrum). Spectra were recorded after white light illumination at 198 K for ~5 s. [Chl] = 1.1 mg·mL^{-1}. Instrument settings: temperature, 8.6 K; modulation amplitude, 25 G; microwave power, 20 mW; microwave frequency, 9.4 GHz; modulation frequency, 100 kHz.

Mn_4CaO_5 measured at 291 nm generated by a sequence of saturating laser flashes. Fig. 3 (upper panels) shows the data generated by a flash sequence in PsbA3-PSII (black), D1/T179I PSII (red), D2/I178T PSII (blue), and D2/I178H-PSII (green) after dark adaptation. At 100 ms after each flash, electron donation from the Mn_4CaO_5 to the $Tyr_Z^{\bullet}$ is complete and the absorption change at 291 nm arises only from changes in the redox state of the Mn_4CaO_5 cluster itself [37].

In the upper Panels of Fig. 3 no significant differences in both the oscillating pattern and the amplitude of the oscillations were observed in the PSII mutants compared to the PsbA3-PSII. This shows that the purified PSII cores are all fully active at room temperature under a saturating flash illumination. Similar results were obtained in the D1/T179H mutant [26].

The formation of the S_2 multiline EPR signal induced by an illumination at 198 K was also monitored in the 3 mutants and compared to that in PsbA3-PSII. The lower Panel in Fig. 3 shows the EPR spectra recorded after a continuous illumination for ~5 s at 198 K in the 3 mutants. In the D1/T179I (red spectrum), the D2/I178T (blue spectrum) and D2/I178H (green spectrum), the S_2 multiline signal is identical and has a comparable amplitude to that in PsbA3-PSII (black spectrum). This shows that the charge separation at 198 K under continuous illumination is equally effective in forming the S_2 state as previously reported for other mutants as the D1/T179H, D1/T179V and D1/H198Q [26]. Therefore, mutations affecting the Chl-*a* molecules constituting the photochemical trap do not perturb the environment of the Mn_4CaO_5 cluster.

The other features in the EPR spectra are all well-known (Fig. 3 lower panel): *i*) The saturated signal centered at ~3385 gauss originated from $Tyr_D^{\bullet}$ [38]; *ii*) The signal at ~2250 gauss is the g_z signal of the oxidized cytochromes (the $Cytc_{550}$ with a small proportion of $Cytb_{559}$) [39]; *iii*) The signal at ~4100 gauss is the $Q_A^-Fe^{2+}Q_B^-$ signal induced in centers in which Q_B^- is present prior to the 198 K illumination. In the other centers, the signal of $Q_A^-Fe^{2+}$ is detected at ~3450 gauss [13]. The presence of these signals in comparable amounts also points to intactness and good comparability between all the samples.

The SDS-polyacrylamide gel electrophoresis (Fig. 4A, the lanes labelled "dark") shows no loss of subunits in PSII from any of the mutants. More detailed explanations of the results in this figure are given later. These results are consistent with the spectroscopic and mechanistic data indicating that the mutants are essentially intact and comparable with each other and the non-mutated strain.

3.2. Flash-induced absorption changes in the Soret region in O_2 evolving PSII

The effects of the mutations on the $P_{680}^+Q_A^-$-*minus*-$P_{680}Q_A$ difference spectrum in the Soret region were measured at room temperature by recording the time-resolved flash-induced absorption changes around 430 nm. In this spectral region, the redox changes of several species, such as the Chls, cytochromes, Tyr radicals and semi-quinones, give rise to absorption changes. These changes also include electrochromic band shifts of pigments in response to the formation of the $P_{680}^+Q_A^-$ state (see *e.g.,* [40] and references therein). Twenty ns after a laser flash the most prominent change is a strong Soret band bleaching around 432 nm that is associated with the formation of $[P_{D1}P_{D2}]^+$ [10]. Fig. 5 shows the absorption changes measured 20 ns after the first flash given to dark-adapted PSII. These spectra therefore corresponded to the to $S_1Tyr_Z[P_{D1}P_{D2}]^+Q_A^-Q_B$-*minus*-$S_1Tyr_Z[P_{D1}P_{D2}]Q_AQ_B$ difference spectrum. In all the mutants, the largest bleaching was between 432 nm and 433 nm for the 4 samples thus indicating that the $P_{D1}^+P_{D2} \leftrightarrow P_{D1}P_{D2}^+$ equilibrium seems hardly affected 20 ns after the flash. In the D1/T179I mutant the spectrum was reproducibly broader on its long-wavelength side between 435 and 445 nm.

Note that the spectral contribution between 440 nn and 460 nm, which has an unknown origin, and discussed in detail in [41], is insensitive to mutations affecting either Chl_{D1} or Chl_{D2}. It is thus unlikely that this feature originates from a band-shift of either Chl_{D1} or Chl_{D2}. It was observed previously [26], at shorter times after the flash (5 ns instead of 20 ns here), that the spectrum was very slightly broaden on the long-wavelength side in the D1/T179H mutant and to the shorter wavelength side in the D1/T179V mutant.

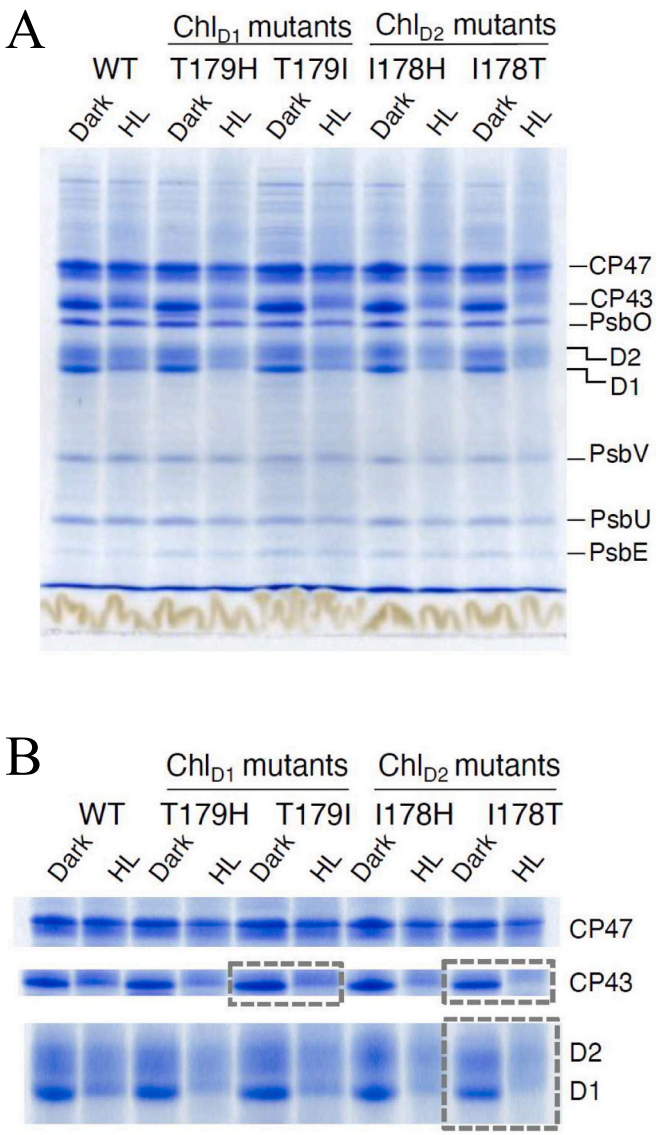

Fig. 4. Panel A: Coomassie brilliant blue-staining of SDS-polyacrylamide gel electrophoresis of dark-adapted and high-light (HL) illuminated PSII samples; PsbA3-PSII (WT), D1/T179H-PSII, D1/T179I-PSII, D2/I178H-PSII and D2/I178T-PSII. Panel B: Edited part of gels showing CP47, CP43, D2 and D1 from Panel A. Squares surrounded by dashed lines indicate bands that degrade significantly under high-light illumination.

3.3. Decay kinetics of $[P_{D1}P_{D2}]^+$ in O_2 evolving PSII

Fig. 6 shows the decay kinetics of $[P_{D1}P_{D2}]^+$ measured at 432 nm after the first flash given to dark-adapted PsbA3-PSII (black), D1/T179I-PSII (red), D2/I178T-PSII (blue) and D2/I178H-PSII (green). In the D2/I178T mutant the multiphasicity in the decay at 432 nm the global $t_{1/2}$ appears to be slightly slower in the 100 ns to 5 μs time range, while at times longer than 5 μs the kinetic are similar in all samples.

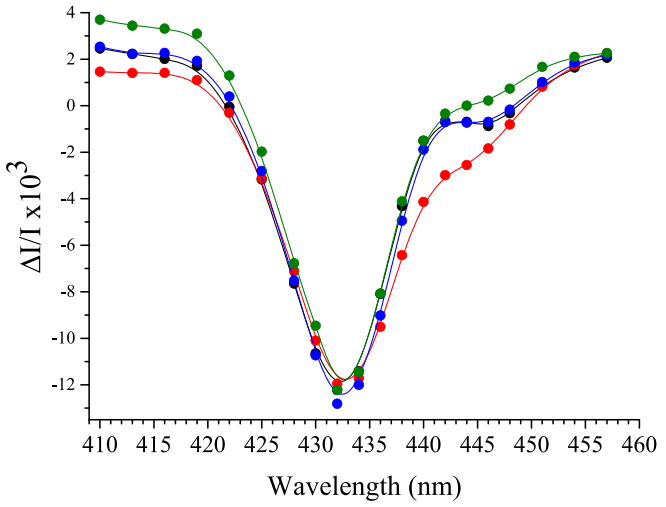

Fig. 5. Light-*minus*-dark spectra recorded 20 ns after the first laser flash illumination given to dark-adapted PSII. Black, PsbA3-PSII; red, D1/T179I-PSII; blue, D2/I178T-PSII; green, D2/I178H-PSII. The spectra were normalized to a Chl concentration of 25 μg mL^{-1}. 100 μM PPBQ was added before the measurements.

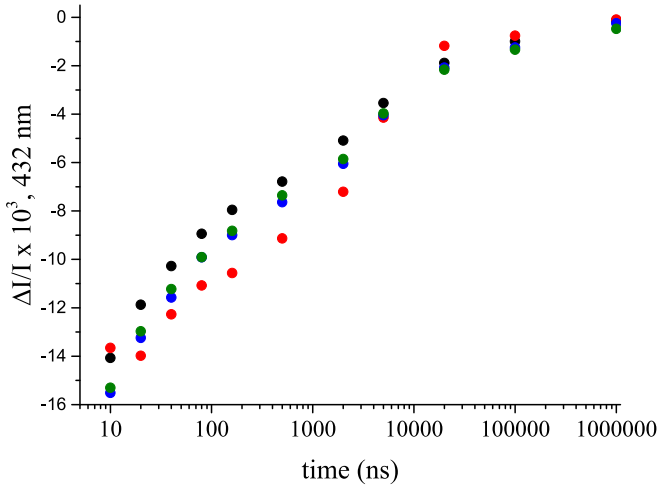

Fig. 6. Kinetics of flash-induced absorption changes measured at 432 nm in PsbA3-PSII (black), D1/T179I-PSII (red), D2/I178T-PSII (blue) and D2/I178H-PSII (green). The amplitudes of the kinetics were normalized to a Chl concentration of 25 μg/ml. 100 μM PPBQ was added before the measurements were taken.

3.4. Thermoluminescence

The intactness of the Mn_4CaO_5 cluster in the mutants studied here makes possible a study of the charge recombination process by thermoluminescence as previously reported [26]. Fig. 7 shows the TL curves resulting from the $S_2Q_A^-$/DCMU charge recombination after 1 flash given at −15 °C in the presence of DCMU. The curves were recorded in PsbA3-PSII (black), D1/T179I-PSII (red), D2/I178T-PSII (blue) and D2/I178H-PSII (green) with a heating rate of 40 °C min^{-1}. For a better comparison with the previous data [26], the TL was measured again in the D1/T179H-PSII (brown curve) in the conditions used for Fig. 7.

In the PsbA3-PSII, the TL signal peaked at ~21 °C for a heating rate of 40 °C min^{-1}. In both the D1/T179I-PSII and D2/I178H-PSII, the amplitude was significantly decreased, whereas the peak temperature was hardly affected. In the D2/I178T-PSII, the TL peak temperature was slightly upshifted to ~23 °C and had an amplitude similar to that in

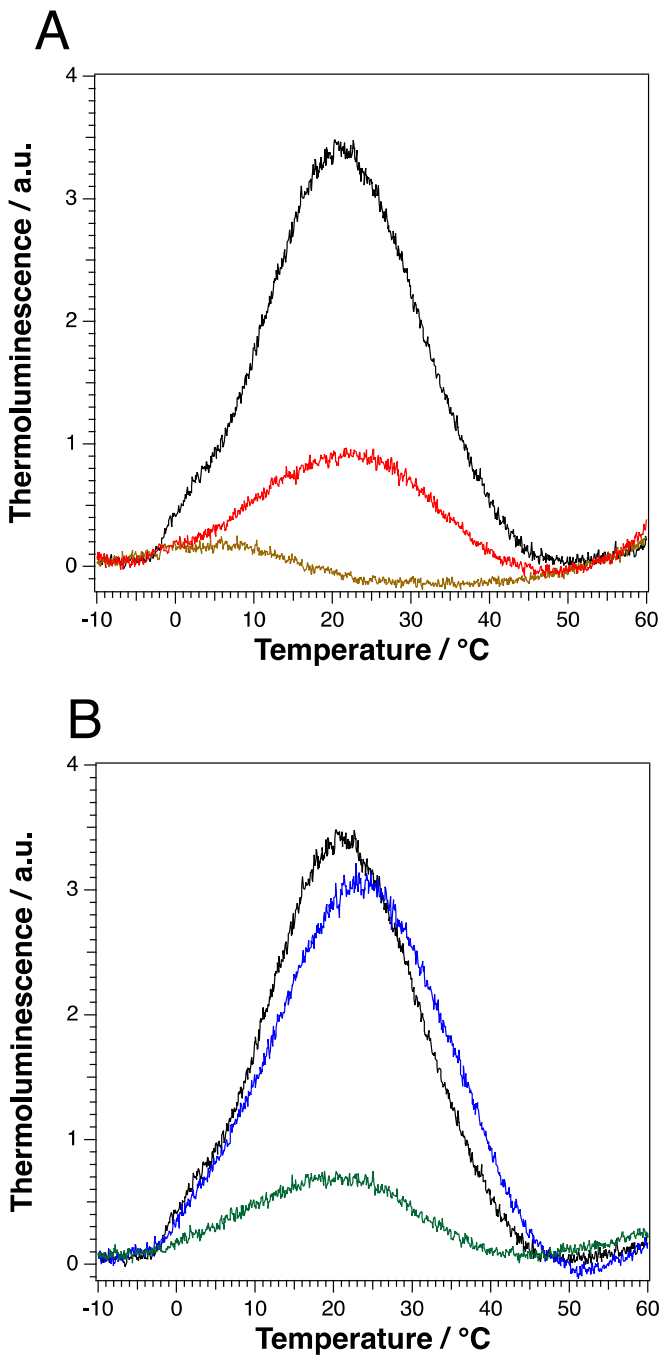

Fig. 7. Thermoluminescence curves from $S_2Q_A^-$/DCMU charge recombination measured after one flash given at −15 °C. Panel A: PsbA3-PSII (black trace), D1/T179I-PSII (red trace), D1/T179H-PSII (brown curve). Panel B: PsbA3-PSII (black trace), D2/I178T-PSII (blue trace), D2/I178H-PSII (green trace). The samples were dark-adapted at room temperature for 1 h prior to the addition of DCMU. The heating rate was 40 °C min^{-1}.

PsbA3-PSII. The TL in the D1/T179H-PSII, as reported earlier [26], had a much lower amplitude and the residual TL peak had a much lower temperature (~ 5 °C).

The amplitude of TL is inversely proportional to the fraction of centres having Q_B^- present in the dark. This reflects the binding of DCMU displacing Q_B from its site when it is transiently formed in the $Q_AQ_B^- \leftrightarrow Q_A^-Q_B$ equilibrium, thereby forming the stable Q_A^-/DCMU state in the dark. Consequently, centres with Q_A^- present in the dark will not be able to form $S_2Q_A^-$ upon excitation. We verified that in the samples studied in Fig. 7, after incubation in the dark for ~1 h, about half of the centers

were in the Q_B^- state based on the amplitude of the EPR $Fe^{2+}Q_B^-$ signal (not shown) but see [13,14,26]. Therefore, the differences in the amplitudes of the TL curves is not due to the initial proportion of Q_B^-. However, the D2/I178T-PSII, did not behave like the other samples; in this mutant the amplitude of the TL peak doubled after 4 h of dark adaptation (see the supplementary material), while in all the other mutants the TL peaks maintained the same amplitude (not shown). Preliminary EPR experiment (see the supplementary material) showed that the decay of Q_B^- in D2/I178T-PSII was possibly slightly faster than in PsbA3-PSII, resulting in higher proportion of open centers after the addition of DCMU.

3.5. The triplet formation

The non-radiative charge recombination process occurs *via* different routes and one of these is the pathway involving the formation of the $^3Chl_{D1}$ triplet state from the $^3[P_{D1}^+Phe_{D1}^-]$ radical pair, *e.g.* [42–44]. We have therefore looked for possible changes in the triplet EPR signals in the mutants. It is necessary to double reduce the quinone Q_A to facilitate the detection of the $^3Chl_{D1}$ [45] this results in a marked increase in the lifetime of $^3Chl_{D1}$ [42]. We have reported previously [26] that at pH values ≥8.0 the amplitude of the triplet EPR signals were much smaller in PsbA3-PSII when compared to what is observed in plant PSII [11,46], but see [42]. Here we found that this was in part due to a greater stability of the Phe_{D1}^- radical in PSII from *T. elongatus* in the presence of dithionite after the double reduction of Q_A. In those centres where Phe_{D1}^- is present in the dark, illumination at 4.2 K does not result in charge separation and consequently $^3Chl_{D1}$ is formed in a lower proportion of centers. Here we increased the redox potential of the dithionite by working at pH 6.5, allowing Phe_{D1}^- to decay and indeed, the triplet EPR signals where much larger. The shape of the spectra in the PsbA3-PSII and D1/T179H-PSII (not shown), were as previously as seen in cyanobacterial PSII [26,42,47].

Fig. 8, upper Panel, compares the triplet EPR signals in PsbA3-PSII (black spectra), in D2/I178T-PSII (blue spectrum) and D1/T179I-PSII (red spectrum).

The triplet signals in the D2/I178T-PSII (and D2/I178H-PSII, not shown) have the same spin polarisation, typical of radical pair recombination [48] and the same splittings (612 gauss typical for chlorophyll *a*) as those of the equivalent triplet in the native PsbA3-PSII. This is attributed to the triplet state localised on Chl_{D1} [11]. In contrast, the spectrum recorded in the D1/T179I-PSII (Fig. 8 upper panel, red spectrum) exhibits two different triplet signals both with similar polarisation patterns but with different splittings. The triplet signal has Z peak splittings (610 gauss) very similar, but not identical, to the classic radical pair recombination Chl_{D1} triplet (612 gauss) (see Fig. 8 lower panel). The slightly narrower Z splitting for what is assumed to be Chl_{D1} triplet in D1/T179I-PSII, was also observed in the D1/T179H-PSII [26].

Fig. 8 shows the triplet signal in D1/T179I-PSII in which the second and broader signal is encircled in the left half of the spectrum. Subtracting the PsbA3-PSII spectrum from the total spectrum to obtain the new triplet signal alone is difficult because as shown in the lower Panel of Fig. 8, that is a zoom of the feature at ~3694 gauss, this band was very slightly shifted in the D1/T179I-PSII as also observed in the D1/T179H-PSII [26]. The ZFS parameters and the polarisation pattern indicate this second triplet is located on a pheophytin and is formed by radical pair recombination [49]. One possibility considered at one time was that during the treatment of PSII to allow the formation of the triplet, Chl_{D1} lost its Mg^{2+} in a proportion of the centres. As the amplitude of the EPR signal of the second triplet is always the same when compared to the $^3Chl_{D1}$ triplet in all the samples studied, this hypothesis seems unlikely. In the literature, triplet with a similar ZFS D parameter was reported as a second minor contaminant in PSII D1/D2 particles [50]. In [50] the lack of resolved X and Y peaks and its lack of response to Phe reduction led to its attribution to contaminating pheophytin formed during the isolation processes.

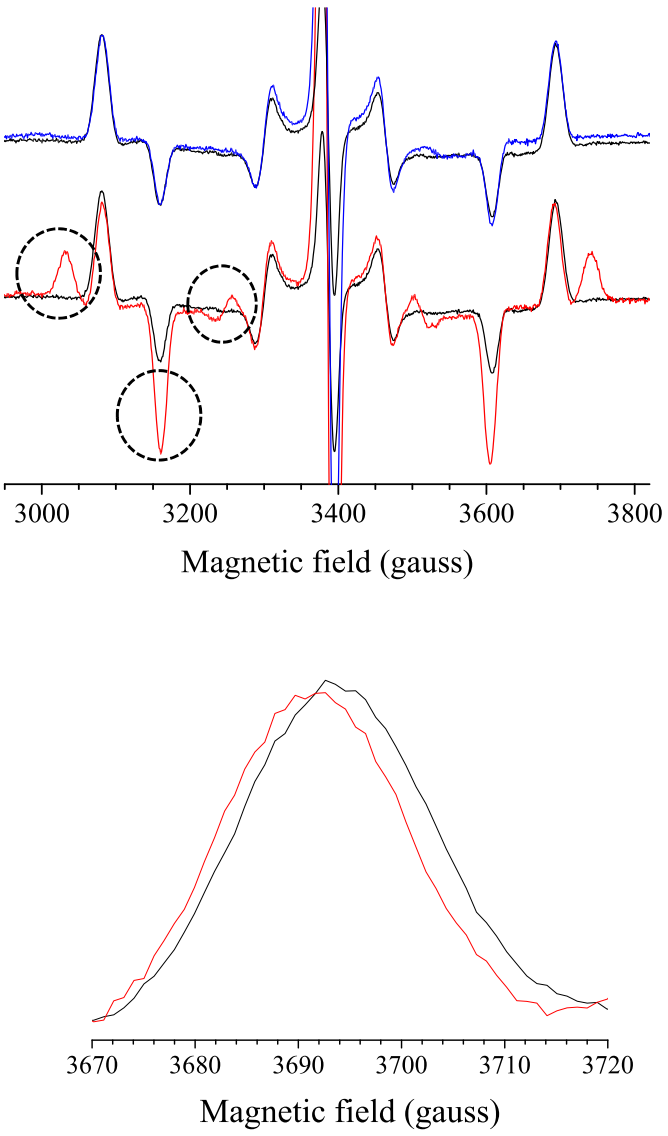

Fig. 8. Triplet EPR signals in PsbA3-PSII (black spectrum), D2/I178T-PSII (blue spectrum) and D1/T179I-PSII (red spectrum). The samples were pretreated with 40 mM dithionite and illumination at room temperature for 5 min followed by dark adaptation for 30 min at room temperature before freezing. Panel A shows the full spectra and Panels B shows the external line at high field with an expended magnetic field scale in PsbA3-PSII (black trace) and D1/T179I-PSII (red trace). The spectra were recorded under continuous illumination at 4.2 K. Instrument settings: modulation amplitude, 25 G; microwave power, 63 μW; microwave frequency, 9.4 GHz; modulation frequency, 100 kHz. The center of the spectra in Panel A corresponds to saturated radical signal.

3.6. Electrochromic band shifts at 77 K in the Qy spectral region upon Q_A^- formation

Fig. 9 shows the electrochromic shifts in Q_Y region of the spectra upon Q_A^- formation at ~77 K in the mutants studied. The D1/T179H mutant, reported earlier [26] is re-measured here for comparison. The blue-shift centered at ~686 nm in PsbA3-PSII was red-shifted by ~3 nm from ~686 nm to ~689 nm in the D1/T179H-PSII as reported earlier [26]. In the D1/T179I-PSII, the blue-shift at ~686 nm was significantly less resolved, showing with a weaker feature at ~686 nm. The 686 nm blue-shift feature was unaffected by the Chl_{D2} mutations. These data indicate that the 686 nm band arises largely from Chl_{D1}. This conclusion agrees with earlier site-directed mutation studies from *Synechocystis* PCC 6803 [9,26,51], from *T. elongatus* [26] and other spectroscopic and

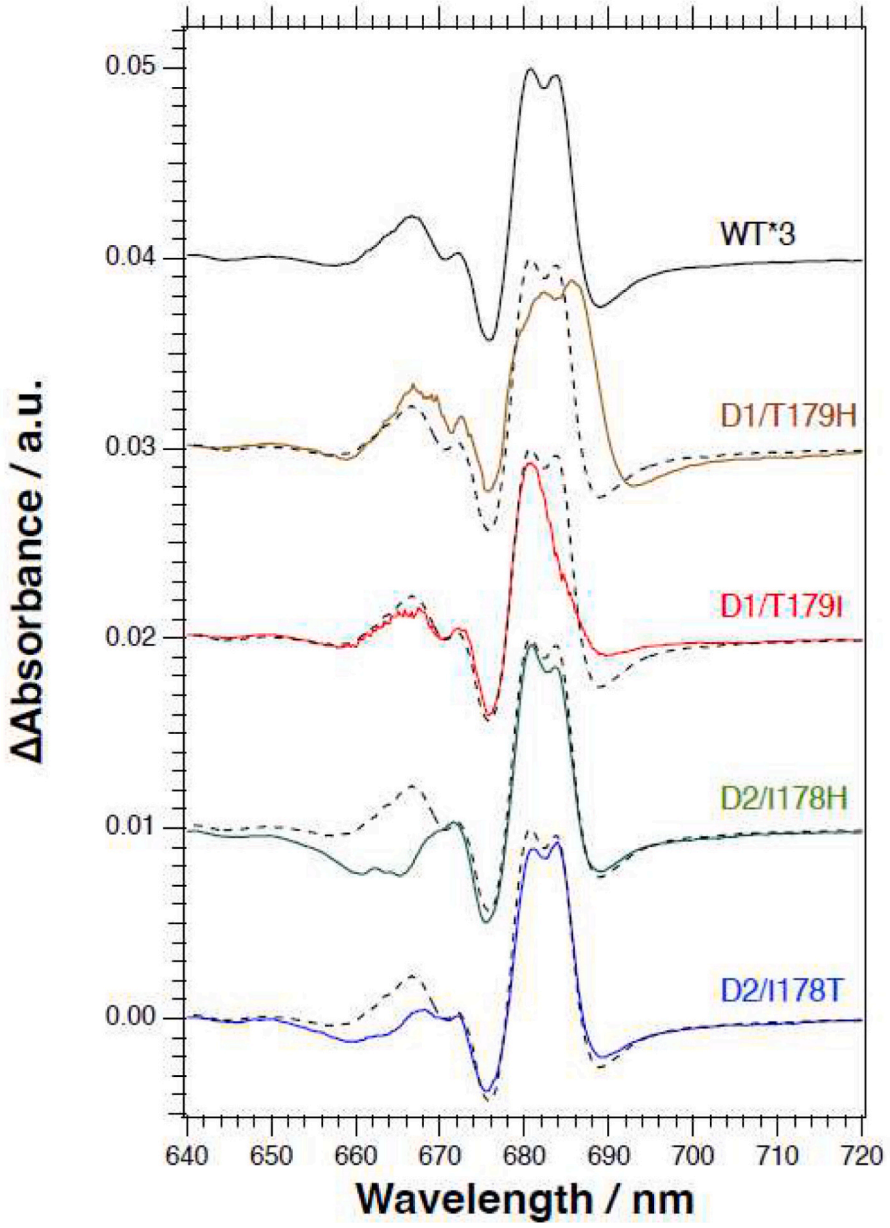

Fig. 9. Light-*minus*-dark difference absorption spectra in the Qy spectral range and recorded at 77 K. After the recording of the spectrum on the dark-adapted samples, illumination at 77 K was given before the recording of the spectrum upon illumination on PsbA3-PSII (black spectrum), D1/T179H-PSII (brown spectrum), D1/T179I-PSII (red spectrum), D2/I178T-PSII (blue spectrum) and D2/I178H-PSII (green spectrum). The dashed lines are the spectrum recorded in PsbA3-PSII.

theoretical work, *e.g.* [10,51–53].

In Fig. 9, the biggest band-shift is the red-shift at 678.6 nm. This feature is not greatly affected by the Chl_{D1} or Chl_{D2} mutations. These observations fit with an assignment to Phe_{D1} and Phe_{D2}. Phe_{D1} has a geometry that makes most susceptible to be red-shifted by Q_A^-, although it often assigned as a shorter wavelength (670 nm [9] to 676 nm [54]), while Phe_{D2} is predicted to give a small red-shift but is thought to have a longer wavelength (678 nm) than Phe_{D1} [9,53–55].

The D1/T179H-PSII with the perturbed Chl_{D1} site showed a small change in the red shift around 678.6 nm, this could reflect the main contribution to this feature from $Phe_{D1,}$ as Chl_{D1} and Phe_{D1} undergo a significant coulombic interaction, so a perturbation of Chl_{D1} could affect Phe_{D1}. The lack of an effect on the red-shift in the two D2 mutations may argue that Phe_{D2} has a minor contribution to this feature if any.

The blue shift feature at 674 nm in Fig. 9 is attributed to the lower of the two separated exciton states (at 660 and 674 nm) resulting from the strongest excitonically coupled chlorophyll pair, $[P_{D1}P_{D2}]$. This confirms earlier site-directed mutagenesis work, in which D1/His198, the axial ligand for P_{D1}, was targeted resulting a shift in the bleach at 672.5 nm upon P_{680}^+ formation in *Synechocystis* PCC 6803 [10,27,51], and in the Q_A^--induced blue-shift at 672 nm in *T elongatus* [26]. The 674 nm part is barely affected in the mutants studied here, although there may be slight shifts (<1 nm) to the red in the two Chl_{D1} mutations.

The shorter wavelength red shift at 669 nm may be attributable to Phe_{D1}, the shorter wavelength of the two Phe's, as this is the wavelength calculated for this pigment by Muh et al. [9]. If correct, this would mean that 678 red shift arises solely from the Phe_{D2} and not a combination of both pheophytins as suggested above. The 669 nm red shift is not visible in the spectra from the two Chl_{D2} mutations but this might be due to overlap with shifts in $Chl_{D2,}$ which is expected to absorb at ~670 nm (see below).

In Fig. 9, the two Chl_{D2} mutations (D2/I1789T and D2/I178H) had

no effect on the band shift at 686 nm compared to the control (PsbA3-PSII), indicating that the mutation near Chl_{D2} does not change the absorption spectrum of Chl_{D1}. The two Chl_{D1} mutations (D1/T179H and D1/T179I) had very little effect on spectral region between 660 nm and 675. In contrast, the weak red shift centred at 663 nm in PsbA3-PSII was shifted by 2 nm to 665.5 nm in D2/I178T-PSII, and by 4 nm to 667 nm in the D2/I178H-PSII upon Q_A^- formation. This result indicated that Chl_{D2} absorption peak is located at 663 nm. This value is at a shorter wavelength than is reported and calculated for Chl_{D2}, *i.e.* 669 nm, in earlier work, *e.g.* [9,52]. The weakness of the shifts and the more marked mismatch with the theoretical values make the assignment of the Chl_{D2} absorption more tentative than the other assignments.

3.7. Singlet $^1O_2$ formation

Since the PSII from mutants with modified Chl_{D1} and Chl_{D2} properties studied are fully active this prompted us to study to what extent these mutations may affect the production of reactive oxygen species, in particular the singlet $^1O_2$ known to be formed by the reaction of $^3O_2$ with $^3Chl_{D1}$. Table 1 reports the production of $^1O_2$ determined by using the protocol described by Rehman et al. [56].

As reported and discussed earlier, the production of $^1O_2$ was slightly smaller in the D1/T179H-PSII mutant when compared to that in PsbA3-PSII. In the D1/T179I-PSII and the D2/I178H-PSII, the $^1O_2$ production were hardly affected when compared to PsbA3-PSII. The most affected mutant was the D2/I178T-PSII, with approximately 3 times more $^1O_2$ produced than in PsbA3 PSII.

3.8. Photoinhibition

It was previously shown that Chl_{D1} was the main chlorin pigment bleached by the $^1O_2$ produced by the reaction of chlorophyll triplet with $^3O_2$ [26]. Since some of the mutants studied here produce much more $^1O_2$ and one shows the triplet localised on a pheophytin in a significant fraction of centres, we have monitored the extent of the bleaching of pigments under high-light illuminations (Fig. 10).

Two of the PSII mutants, the D1/T179I-PSII and the D2/I178T-PSII, were severely affected by the high-light illumination; while the D2/178H-PSII has a slight increase in bleaching. These three mutants are the top three $^1O_2$ generators (Table 1) but this correlation is not quantitative. The D2/I178T-PSII, with its rate of $^1O_2$ production being 3 times that of the control, correlates quite well with the largest bleaching, which is ~2.6 times the bleaching seen in the control. However, the D1/T178I-PSII showed only ~1.2 times higher rate of $^1O_2$ production but has 2.2 times the bleaching of the control. This discrepancy could indicate a different origin of the bleaching, or it could reflect the different illumination conditions used for the two measurements: $^1O_2$ generation rate used very high-light for a short time, while the bleaching experiment used 4 times lower intensity but for 1 h.

The CBB staining of SDS-polyacrylamide gel shown shown in Fig. 4 for PSII after being exposed to a high intensity illumination shows that the CP43, D2 and D1 contents decreased similarly in all the mutants when compared to PsbA3-PSII, except for the D2/I178T-PSII mutant, in which this decrease was much more marked. This result agrees well with the stronger pigment bleaching observed in this mutant.

Table 1
Singlet oxygen production by PSII under high-light (20,000 μmol photons m^{-2} s^{-1}).

Strain	$^1O_2$ production μmol $^1O_2$ (mg Chl)$^{-1}$ h^{-1}	Relative %
PsbA3-PSII	123 ± 2.2	100 %
D1/T179H	89.2 ± 2.4	72 %
D1/T179I	143 ± 2.7	116 %
D2/I178H	130 ± 3.6	106 %
D2/I178T	358 ± 5.7	291 %

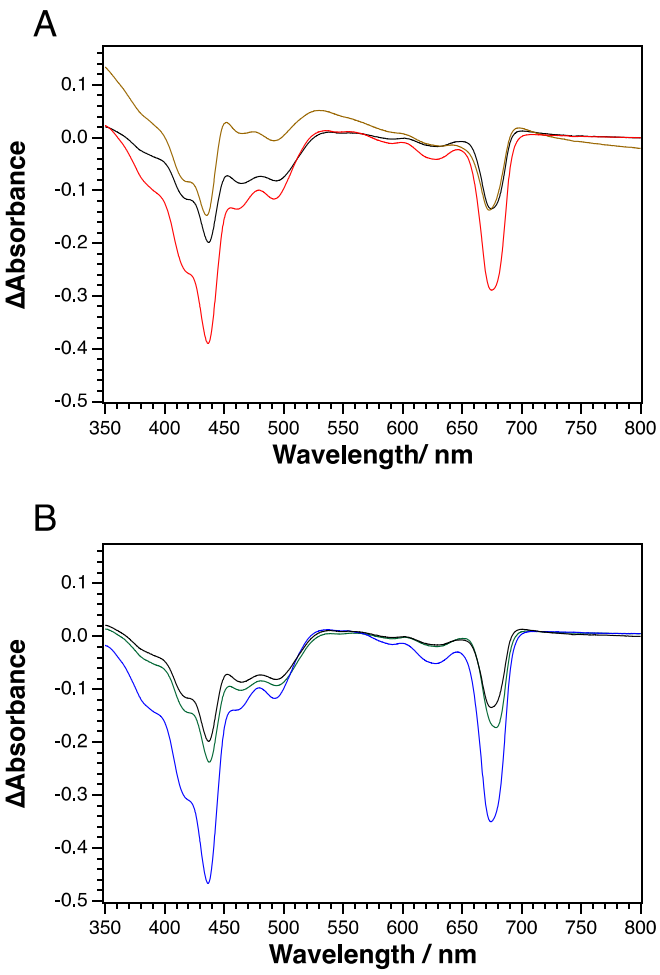

Fig. 10. Difference spectra between 350 and 800 nm recorded at room temperature in PsbA3-PSII (black spectrum), D1/T179H-PSII (brown spectrum), D1/T179I-PSII (red spectrum), D2/I178T-PSII (blue spectrum) and D2/I178H-PSII (green spectrum). The samples were illuminated at 45 °C for 60 min under a light intensity of ~500 μmol photons m^{-2} s^{-1}.

Radical formation was searched for after high-light illumination by performing an immunoblot analysis against DMPO which forms an adduct when a radical is induced in a protein, *e.g.* [33], Fig. 11.

Fig. 11 shows that, as expected, upon an incubation in the dark in the presence of DMPO, the immunoblot revealed no radical formation. Under high-light conditions, the extent of radical formation was less in the D1/T179H-PSII and the D2/I178H-PSII than in PsbA3-PSII. For the

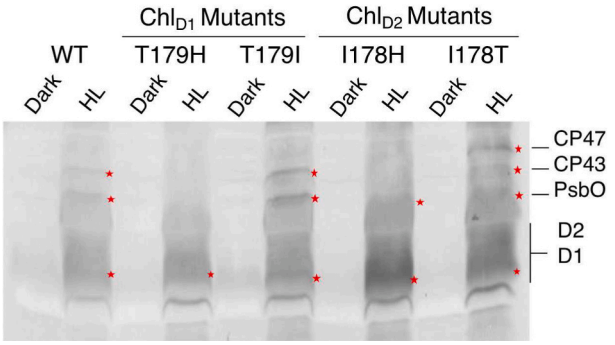

Fig. 11. Immunoblot analysis of PsbA3-PSII, D1/T179H-PSII, D1/T179I-PSII, D2/I178H-PSII and D2/I178T-PSII samples labelled with DMPO. The detection was done using anti-DMPO antibodies.

D1/T179H-PSII, the result agrees with what we saw before with this mutant (a smaller bleaching and a smaller $^1O_2$ production [26] and data above). In the D1/T179I-PSII, the labelling was slightly larger than in PsbA3-PSII for CP43 and PsbO. For CP43 this is in agreement with the larger bleaching increased $^1O_2$ observed above in this mutant (Table 1 and Fig. 10). Fig. 11 shows that the D2/I178T-PSII is the mutant the most affected by high intensity illumination, showing radical formation in all the major PSII subunits, and this correlates well with its greater susceptibility photodamage (Fig. 4), photobleaching (Fig. 11) and $^1O_2$ formation (Table 1).

4. Discussion

The aim of the present work was to characterise the influence of the immediate protein environment on the properties of Chl_{D1} and Chl_{D2}. For that, several site-directed mutants were constructed focussing on the amino acids close to the water molecule that acts as the axial ligand to the Mg^{2+} in each of these chlorophylls. In Chl_{D1}, which is thought to act as the primary electron donor, the key amino acid is D1/T179, while its symmetrical counterpart associated with Chl_{D2} is D2/I178. These highly conserved amino acids likely contribute to the functional differences: Chl_{D1} is the primary donor, while Chl_{D2} does not seem to play a direct role in charge separation. Here the T to I swap in D_1 may be expected to make Chl_{D1} more Chl_{D2}-like, while the I to T swap in D_2 could make Chl_{D2} more like the primary donor. The main effects of these mutations are summarized in Table 2 and discussed below.

The main bleach in the Soret region (Fig. 5), which is associated with chlorophyll cation formation, and considered to be mainly due to P^+_{D1} with a potential contribution from P^+_{D2}, was found *i*) to be unchanged in three of the four mutants investigated here, D1/T179H-PSII, D2/I178T-PSII and D2/I178H-PSII, compared with the control strain, PsbA3-PSII, and *ii*) to show only a minor change in the D1/T179I mutant (see below). This finding indicates that P^+_{D1} remains largely unaffected by the mutations, in terms of its spectrum and the dominant location of the cation, at least in the tens of ns time-range after charge separation.

In the D1/T179I mutant, however, there is a minor additional bleaching detectable between 440 and 445 nm. The D1/T179I mutation changes the hydrogen bonding environment of the water that is the axial ligand for the Mg^{2+} in Chl_{D1}. Such a perturbation could influence the pigments adjacent to Chl_{D1}, particularly those to which it is most strongly coupled. P_{D2} and Phe_{D1} are calculated to have the strongest couplings to Chl_{D1} (− 47 and 44 cm^{-1}, respectively), while its coupling to P_{D1} is significantly smaller (− 27 cm^{-1}), see [9]. The additional bleaching at 440–445 in D1/T179I-PSII could thus reflect a small perturbation of the cation distribution ($P^+_{D1}P_{D2} \leftrightarrow P_{D1}P^+_{D2}$) or a change in the environment of P_{D2} due to a change in the Chl_{D1}-P_{D2} coupling in the mutant [10].

The 77 K difference spectra of the mutants showed only slight changes, in the Chl_{D1} mutations, or no changes, in the Chl_{D2} mutations, in the blue-shift attributed to P_{D1}/P_{D2} at 674 nm (Fig. 9). These data confirm that the absorption spectrum of P_{D1}/P_{D2} is largely unaffected by mutations close to Chl_{D1} and Chl_{D2}.

The D1/T179I mutant that shows the most chlorophyll bleaching after illumination with high-light intensity (Fig. 10), is also the most modified in terms of its chlorophyll EPR triplet signals (Fig. 8). This mutant shows 2 different triplets: a typical radical pair recombination triplet from monomeric Chl-*a* [48], and a second triplet, also with a typical radical pair recombination polarisation pattern, but with a splitting indicative of a pheophytin [49]. The most straightforward explanation for the additional triplet is that the perturbation of the Chl_{D1} resulted in a significant fraction of the triplet being localised on the Phe_{D1}. It was suggested previously that the triplet on Chl_{D1} migrates at low temperatures onto the Phe_{D1}, there to be quenched by Q_A^- in an electron transfer process [42,57]. This was suggested to explain the anomalously rapid decay of the triplet when Q_A^- is present [42,57]. The present work may represent direct experimental evidence for triplet transfer from Chl_{D1} to Phe_{D1} and potentially for the quenching model.

Table 2
main observations made on the 4 mutants PSII; D1/T179I-PSII, D1/T179H-PSII, D2/I178T-PSII and D2/I178H-PSII.

	D1/T179I-PSII[a]	D1/T179H-PSII[a,b]	D2/I78T-PSII[a]	D2/I78H-PSII[a]
Period 4 at 291 nm	~ PsbA3-PSII	~ PsbA3-PSII	~ PsbA3-PSII	~ PsbA3-PSII
S_2 multiline EPR	amplitude and shape ~ PsbA3-PSII	amplitude and shape ~PsbA3-PSII	amplitude and shape ~PsbA3-PSII	amplitude and shape ~PsbA3-PSII
Soret ΔA $[P_{D1}P_{D2}]^+$	432 nm ~ PsbA3-PSII, broader on long λ side	432 nm ~ PsbA3-PSII, broader on long λ side	432 nm ~ PsbA3-PSII	432 nm = PsbA3-PSII
Decay $[P_{D1}P_{D2}]^+$	slower in 0.1–1 μs range	~ PsbA3-PSII	~ PsbA3-PSII	~ PsbA3-PSII
TL $S_2Q_A^-$/DCMU	T ≤ PsbA3-PSII, ampl. << PsbA3-PSII	T < PsbA3-PSII, ampl. << PsbA3-PSII	T = PsbA3-PSII, ampl. ~ PsbA3-PSII	T < PsbA3-PSII, ampl. << PsbA3-PSII
Triplet EPR signal	2 triplets, 1 ~ PsbA3-PSII 1 = pheophytin ($^3Phe_{D1}$?)	~ PsbA3-PSII	~ PsbA3-PSII	~ PsbA3-PSII
Chl_{D1} band shifts (Qy)	smaller than PsbA3-PSII λ as PsbA3-PSII	λ red-shifted by ~3 nm	ampl. ~ PsbA3-PSII, λ ~ PsbA3-PSII	ampl. ~ PsbA3-PSII, λ ~ PsbA3-PSII
Chl_{D2} band shifts (Qy)	ampl. and λ ~ PsbA3-PSII	ampl. ~ PsbA3-PSII λ ~ PsbA3-PSII	ampl. ~ PsbA3-PSII, λ red-shifted by 2 nm	ampl. ~ PsbA3-PSII, λ red-shifted by 4 nm
$^1O_2$ production	≥ PsbA3-PSII	decreased by ~10–30 %	> > PsbA3-PSII	~ PsbA3-PSII
Bleaching HL 680 nm	~ 2.2 x PsbA3-PSII	ampl. ~ PsbA3-PSII λ slightly red-shifted	~2.5 x PsbA3-PSII	~ 1.3 x PsbA3-PSII
degraded proteins under high light > PsbA3-PSII	CP43	CP43	CP43, PsbA, PsbD	CP43?
oxidized proteins under high light > PsbA3-PSII	PsbA, PsbO, CP43	PsbA	PsbA, PsbO, CP47, CP43	PsbA

ampl. = amplitude.
[a] This work.
[b] This work and ref. [26].

The decay rate of the $[P_{D1}P_{D2}]^+$ state by electron donation from Tyr_Z is also similar in the PsbA3-PSII control and the D1/T179H (not shown), D2/I178H and D2/I178T mutants (Fig. 6). In contrast, the D1/T179I mutant exhibits small but significant differences in the kinetics, with a slowdown of the 10–20 ns phase contributing to a slower overall $t_{1/2}$ value of ~1 μs in D1/T179I-PSII, compared to ~200 ns in PsbA3-PSII and the other mutants. The slowdown in this time range is reminiscent of that observed in the D1/R323E mutant [31], where D1/R323 is part of the H-bond network connecting Tyr_Z to the bulk and suggested to be involved in proton egress, although the effect on the kinetics is less pronounced in the current mutant. This time-range was proposed to correspond in part to a dielectric relaxation stabilizing the Tyr_Z^{ox} initially formed by lowering its free energy level [20,58]. In the present case, it seems unlikely that the H-bond network around Tyr_Z is altered by the D1/T179I mutation, and therefore the slower reduction rate of the $[P_{D1}P_{D2}]^+$ is more likely due to a perturbation arising from a redox or structural effect on $[P_{D1}P_{D2}]^+$ from the modified Chl_{D1}, potentially due to a change in its coupling with P_{D2}.

The lower $S_2Q_A^-$/DCMU TL amplitude in the D1/T179I-PSII mutant, when compared to the PsbA3-PSII (Fig. 7), could result from a larger

energy gap between *Chl_{D1} and the $Chl^{+}_{D1}Phe^{-}_{D1}$ radical pair. The $S_2Q^{-}_{A}$ TL peak is at almost the same temperature (~ 23 °C) as in PsbA3-PSII (~ 21 °C), so the overall energetics of the recombination the $S_2Q^{-}_{A}$ in PsbA3-PSII is not greatly affected in the mutant compared to the control. A lower energy level for the $Chl^{+}_{D1}Phe^{-}_{D1}$ radical pair, without shifting the overall bioenergetics of charge recombination, could arise from a lower potential for the Chl^{+}_{D1}/Chl_{D1} couple and this, in principle, could slow down the decay at 432 nm by shifting the equilibria, $Tyr_ZP_{D1}Chl^{+}_{D1}$ ↔ $Tyr_ZP^{+}_{D1}Chl_{D1}$ ↔ $Tyr^{\bullet}_Z(H^{+})P_{D1}Chl_{D1}$, to the left.

While the change in the energy level of the $Chl^{+}_{D1}Phe^{-}_{D1}$ radical pair may explain the TL and P^{+}_{D1} reduction kinetics, it is insufficient to explain all the properties of the D1/T179I-PSII mutant. The additional properties include: *i*) additional bleaching in the Soret region (Fig. 5); *ii*) the small amplitude of the Chl_{D1} electrochromic shift at 77 K upon Q^{-}_{A} formation (Fig. 9); and *iii*) the appearance of the pheophytin triplet (Fig. 8). As suggested above, these features may arise from changes in electronic coupling between Chl_{D1} and its adjacent cofactors, P_{D2} and Phe_{D1}.

Although the D1/T179I mutant has a different triplet composition, the production of $^1O_2$ under high-light conditions is only slightly (1.2 times) larger than that in the PsbA3-PSII control. However, the chlorophyll bleaching was double that in the PsbA3-PSII control, the CP43 seemed significantly more degraded, and the PsbA, PsbO and CP43 were also oxidized. This mismatch between the amount of $^1O_2$ and the level of photodamage could be related to different conditions used for the measurement of the rate $^1O_2$ formation compared to those used for the photobleaching experiments. However, it is also possible that the discrepancy between the $^1O_2$ and bleaching indicates a true mechanistic difference in the photodamage occurring. The mechanistic difference could involve a change from back-reaction chlorophyll triplet mediated $^1O_2$, to direct over-oxidation of the pigments. If the main pigment bleached by $^1O_2$ produced under high-light by the reaction between $^3Chl_{D1}$ and $^3O_2$ is Chl_{D1} [26], the localisation of the triplet may vary, discussed in [26], and there is a distribution in the localisation of the triplet at room temperature [10,59] so that this reaction may occur in different places.

The electrochromic band shift at 77 K caused by Q^{-}_{A} formation, which is centered at 663 nm in PsbA3-PSII, was red-shifted by 2 nm to 665 nm in the D2/I178T-PSII and by 4 nm to 667 nm in the D2/I178H-PSII. This result indicates that the absorption of Chl_{D2} is somewhat lower that its assignment, 669–670 nm, in earlier theoretical work [9,52]. However, the small red-shift of the absorption of Chl_{D2} upon Q^{-}_{A} formation is consistent with the structure [9,54].

The electrochromic band shift at 77 K upon Q^{-}_{A} formation is also red-shifted by changing its neighbouring isoleucine 178 to either threonine or histidine (Fig. 9). Apart from this small effect in the absorption of Chl_{D2} in the D2/I178T-PSII, several of its other properties are unaffected: *i.e.*, its TL, the decay of P^{+}_{D1}, and the triplet EPR signal are hardly affected in this mutant. This is not particularly surprising as the Chl_{D2} is not thought to play a direct redox role in the main pathway of charge separation and electron transfer. It is thus quite striking that the $^1O_2$ production, the bleaching at 680 nm and the degradation of CP43, PsbA and PsbD, and the oxidation of several proteins are all greatly enhanced under high-light conditions in this mutant. This suggests that Chl_{D2} plays and important role in the reactions leading to and/or protecting against photodamage (see below).

In contrast to the enhanced $^1O_2$ production, bleaching and protein degradation seen in D2/I178T mutant, the D2/I178H mutant showed a level of $^1O_2$ production very similar to that in PsbA3-PSII control (Table 1). The Chl_{D2} absorption in the D2/I178H mutant is red-shifted by 4 nm compared to the PsbA3-PSII control and by 2 nm in the D2/I178T mutant, so both mutants are physically perturbed by their modifications but only D2/I178T has a greatly enhanced susceptibility to photodamage.

The D2/I178H mutant shows other intriguing properties. Modifying the environment of the Chl_{D2} by replacing the D2/Ile178 with an His residue, results in diminished thermoluminescence (Fig. 7). This could be due to a change in the energetics of the central pigments resulting in a decrease in the radiative route, such as an increase in the energy gap between the radical pair that is the immediate precursor of the luminescent state. This however would seem surprising as the Chl_{D2} had little effect on charge separation and the subsequent electron transfer steps, in agreement with its location and previous experimental evidence. However, these TL data suggest that a mutation affecting Chl_{D2} could play a significant role in the charge recombination processes.

Calculations based on the structure of PSII indicate that Chl_{D2} is mainly coupled to its adjacent cofactors: Phe_{D2} and P_{D1} [9,60] with couplings that are slightly weaker (~ 42 cm^{-1}) than for the symmetrical couplings around Chl_{D1} (47 and 43 cm^{-1} to P_{D2} and Phe_{D1} respectively). In the D2/I178H mutant, the modification may have perturbed P_{D1} in way that disfavours the repopulation of the radical pair, $Chl^{+}_{D1}Phe^{-}_{D1}$, that is thought to be the precursor of the luminescent state, *Chl_{D1}. This perturbation could occur by a change in the coupling, through environmental or structural changes, resulting in modifications the redox potentials of P_{D1} relative to that of Chl_{D1} and/or to P_{D2}. Such a perturbation could favor *i*) non-radiative recombination, or *ii*) electron donation from the side-pathway donation route that is initiated by β-carotene oxidation on the D_2 side [61,62]. Electron donation from this pathway has been suggested to be *via* the Chl_{D2}, and even a small redistribution of the cation radical onto Chl_{D2} from P^{+}_{D1} could greatly accelerate electron donation from the β-carotene [4,25] at the expense of charge recombination.

The D2/I178T mutant, which represents the "Chl_{D1}-ification" of the Chl_{D2}, could convert the Chl_{D2}, which seems to have evolved a true "accessory" role, into a Chl_{D1}-type "primary donor" role. This could mean $Chl^{+}_{D2}Phe^{-}_{D2}$ charge separation occurring adventitiously within the reaction centre. Even if this occurred in a low yield and under conditions where Q^{-}_{A} was present (*i.e.*, with "closed centres"), it would likely result in more triplet-mediated $^1O_2$ formation, and likely in a location different from that the usual pathways of $^1O_2$ generation, away from the existing protective processes. This could account for the significant increase in singlet $^1O_2$ formation and the more extensive photodamage in this mutant.

If a role for Chl_{D2} in wild type PSII is to facilitate side-path electron donation, a process that has been rationalised as a protective mechanism [62,63], the D2/I178T mutant may affect this pathway. If so, this too could contribute to the enhanced photodamage. The efficiency of this side-pathway is worthy of study in the Chl_{D2} mutants. The idea that the D2/I178T mutant confers some properties of the primary donor on Chl_{D2}, may also explain the observation that Q^{-}_{B} is unusually (uniquely?) more unstable in this mutant. Q^{-}_{B} is thermodynamically stable [15] and its lifetime is determined by the availability of a sufficiently unstable electron hole on the electron donor side of PSII. When Q^{-}_{B} is formed in the presence of the S_2 or S_3 charge accumulation states of the Mn_4O_5Ca cluster, it decays in tens of seconds by a back-reaction that includes $S_2Q^{-}_{A}$ (or $S_3Q^{-}_{A}$) as an intermediate [64]. But when Q^{-}_{B} is present with the stable charge accumulation states, S_0 or S_1, it is stable for hours [64]. A slow decay (many hours) of Q^{-}_{B} has been reported and this may occur by recombination with $Tyr^{\bullet}_{D}$, *e.g.* [13,62] as there is some experimental evidence that slow $Tyr^{\bullet}_{D}Q^{-}_{A}$ recombination can occur [65]. The unusual slight acceleration of the slow decay of Q^{-}_{B} in the D2/I178T mutant reported here, could be due the existence of a new recombination route arising from the mutation. This could involve electron transfer from Q^{-}_{B} directly to Phe_{D2}, and electron hole transfer from an oxidized donor, such as $Tyr^{\bullet}_{D}$, to P_{D1}/P_{D2} and to Chl_{D2}, allowing charge recombination to occur in $Chl^{+}_{D2}Phe^{-}_{D2}$. However, the decay of $Tyr^{\bullet}_{D}$ seemed not significantly faster in the mutant. This back reaction pathway could reflect what existed in the homodimeric ancestor and in less asymmetric ancestors of PSII before the current asymmetry evolved, resulting in the current more efficient heterodimeric version of PSII [4,66]. This recombination route may exist in wild type PSII but may be too slow to be significant or detectable, but with the putative stronger coupling

between Chl_{D2} and Phe_{D2}, due to the mutation that makes Chl_{D2} more like Chl_{D1}, this recombination route is worth considering explaining the more rapid Q_B^- decay in the D2/I178T mutant.

5. General conclusion

Modifying the key amino acids in the vicinity of Chl_{D1} and Chl_{D2} had little effect on overall enzyme function, charge separation, nor forward electron transfer. The absence of major effects indicates that the specialized function of Chl_{D1} is not due to a single amino acid. This is not a big surprise. Earlier calculations, based on the structure of PSII, compared Chl_{D1} and Chl_{D2} and their protein environments and concluded that the electrostatic asymmetry in PSII, an important property for function, is determined by many small contributions from a wide range of structural elements [9]. A similar conclusion can be drawn here to explain the relative insensitivity of PSII function to the mutations made here.

The robustness of PSII function to mutations also agrees with earlier analysis of PSII function and energetics [25]. That analysis showed that forward electron transfer reactions were rather insensitive to external conditions and to redox tuning [25]. In contrast, back reactions, electron leaks and photodamage were very sensitive to the environment and were controlled by a range of sensitive, redox-tuning-dependent, regulatory, and protective mechanisms [25]. That analysis was reinforced by a series of studies since that time, *e.g.*, the mechanism of photodamage in fluctuating light [67], and the limitations of oxygenic photosynthesis in far red light [24,68,69]. In the present work, the replacement of the conserved D1 threonine with an isoleucine (D1/T179I) that is conserved in D2 in the symmetrical position, has significant effects on back-reactions and protection/photodamage. When the inverse swap was done (D2/I178T), it resulted in even more $^1O_2$ formation and more photodamage. This could arise from D2-side charge separation, which becomes significant under conditions where electron transfer is blocked under high-light. This putative new charge separation ability may open-up a slow charge recombination route down the D2 side of the reaction centre, constituting a new decay route for Q_B^-. This additional charge separation activity may represent the first experimental signs of the original charge separation route that was present in the homodimeric ancestor and in the early heterodimeric ancestors that existed before evolution fully extinguished the D2 charge separation route.

The evolution of the purple bacterial reaction centre is also considered to have involved the conversion of an ancestral homodimeric Type II reaction centre into a heterodimeric Type II reaction centre. The ancestral homodimer did charge separation on both sides of the dimer while the existing heterodimeric reaction centre has charge separation only on one side. The changes that resulted in the shut-down of charge separation in the now non-functional side of the purple bacterial reaction centre have been the focus of many detailed studies, *e.g.* [70–73]. Many of these changes have been elucidated by engineering in features from symmetrical locations on the functional side, resulting in the reactivation of charge separation on "non-functional" side.

Given the marked similarities between purple bacterial reaction centres and PSII [4], it is likely they share some comparable features responsible for the evolutionary of two-sided to one-sided charge separation. However, at a more detailed level, many differences are expected, as these changes are considered to have occurred separately by convergent evolution [74], in which similar selection pressures on two different homodimers, a proto-PSII and proto-purple reaction centre, led to different evolutionary solutions both converging on functionally one-sided heterodimers. As a result, the symmetry swapping experiments that have been done in PSII involve changes that do not correspond closely to those done in the purple bacteria, [70–73] and the present work.

It has been noted [4,25] that Chl_{D2} is the closest reaction centre chlorin to the D2-side β-carotene that is thought to act as the first donor of the protective side pathway [61]. This led to the suggestion that electron donation from the side-path occurs *via* Chl_{D2} [4]. This mechanism presupposes that at least fraction of the positive charge that is mainly localised on P_{D1} and shared with P_{D2} [10] is distributed out to Chl_{D2}; this seems possible and even switchable [4,25]. The modification of the Chl_{D2} by the mutations looked at here may perturb this role. The D2/I178H mutant may show lower radiative recombination due to enhanced side-path donation (and more cation on Chl_{D2}), while other mutant may have less cation from $[P_{D1}/P_{D2}]^+$ distributed over to Chl_{D2}, and thus less side-path donation.

This work provides a basis for future studies aimed at understanding the evolution of the heterodimeric PSII and what controls electron transfer and back reactions on the D2 side, and the evolution and role of the side pathway as a putative protective mechanism.

Declaration of competing interest

The authors declare that they have no known competing financial interests or personal relationships that could have appeared to influence the work reported in this paper.

Data availability

Data will be made available on request.

Acknowledgements

This study was supported by the JSPS-KAKENHI Grant in Scientific Research on Innovative Areas JP17H064351 and a JSPS-KAKENHI Grant 21H02447. AWR was supported by the Leverhulme Trust Research Project Grant RPG-2022-203. AWR thanks Andre Fantuzzi, Geoff Davis and Kenta Renard for useful discussion. AB was supported by the French Infrastructure for Integrated Structural Biology (FRISBI) ANR-10-INBS-05. JS was supported by the Labex Dynamo (ANR-11-LABX-0011-01).

Appendix A. Supplementary data

Supplementary data to this article can be found online at https://doi.org/10.1016/j.bbabio.2023.149013.

References

[1] Y. Umena, K. Kawakami, J.-R. Shen, N. Kamiya, Crystal structure of oxygen-evolving photosystem II at a resolution of 1.9 angstrom, Nature 473 (2011) 55–60, https://doi.org/10.1038/nature09913.
[2] M. Suga, F. Akita, K. Hirata, G. Ueno, H. Murakami, Y. Nakajima, T. Shimizu, K. Yamashita, M. Yamamoto, H. Ago, J-R. Shen, Native structure of photosystem II at 1.95 angstrom resolution viewed by femtosecond X-ray pulses, Nature 517 (2015) 99–103. doi:https://doi.org/10.1038/nature13991.
[3] T. Mirkovic, E.E. Ostroumov, J.M. Anna, R. van Grondelle, Govindjee, G.D. Scholes, Light absorption and energy transfer in the antenna complexes of photosynthetic organisms, Chem. Rev. 117 (2017) 249–293, https://doi.org/10.1021/acs.chemrev.6b00002.
[4] T. Cardona, A. Sedoud, N. Cox, A.W. Rutherford, Charge separation in photosystem II: a comparative and evolutionary overview, Biochim. Biophys. Acta 1817 (2012) 26–43, https://doi.org/10.1016/j.bbabio.2011.07.012.
[5] A.R. Holzwarth, M.G. Müller, M. Reus, M. Nowaczyk, J. Sander, M. Rögner, Kinetics and mechanism of electron transfer in intact photosystem II and in the isolated reaction center: pheophytin is the primary electron acceptor, Proc. Natl. Acad. Sci. U. S. A. 103 (2006) 6895–6900, https://doi.org/10.1073/pnas.0505371103.
[6] E. Romero, V.I. Novoderezhkin, R. van Grondelle, Quantum design of photosynthesis for bio-inspired solar-energy conversion, Nature 543 (2017) 355–365, https://doi.org/10.1038/nature22012.
[7] Y. Yoneda, E.A. Arsenault, S. Yang Jr., K. Orcutt, M. Iwai, G.R. Fleming, The initial charge separation step in oxygenic photosynthesis, Nat. Commun. 13 (2022) 2275, https://doi.org/10.1038/s41467-022-29983-1.
[8] M. Capone, A. Sirohiwal, M. Aschi, D.A. Pantazis, I. Daidone, Alternative fast and slow primary charge-separation pathways in photosystem II, Angew. Chem. Int. Ed. 62 (2023), e202216276, https://doi.org/10.1002/anie.202216276.
[9] F. Müh, M. Plöckinger, T. Renger, Electrostatic asymmetry in the reaction center of photosystem II, J. Phys. Chem. Lett. 8 (2017) 850–858, https://doi.org/10.1021/acs.jpclett.6b02823.

[10] B.A. Diner, E. Schlodder, P.J. Nixon, W.J. Coleman, F. Rappaport, J. Lavergne, W.F. J. Vermaas, D.A. Chisholm, Site-directed mutations at D1-His198 and D2-His197 of photosystem II in *Synechocystis* PCC 6803: sites of primary charge separation and cation and triplet stabilization, Biochemistry 24 (2001) 9265–9281, https://doi.org/10.1021/bi010121r.

[11] F.J.E. van Mieghem, K. Satoh, A.W. Rutherford, A chlorophyll tilted 30° relative to the membrane in the photosystem II reaction Centre, Biochim. Biophys. Acta 1058 (1991) 379–385, https://doi.org/10.1016/S0005-2728(05)80134-3.

[12] H. Tamura, K. Saito, H. Ishikita, Acquirement of water-splitting ability and alteration of the charge-separation mechanism in photosynthetic reaction centers, Proc. Natl. Acad. Sci. U. S. A. 117 (2020) 16373–16382, https://doi.org/10.1073/pnas.2000895117.

[13] C. Fufezan, C.-X. Zhang, A. Krieger-Liszkay, A.W. Rutherford, Secondary quinone in photosystem II of *Thermosynechococcus elongatus*: Semiquinone-iron EPR signals and temperature dependence of electron transfer, Biochemistry 44 (2005) 12780–12789, https://doi.org/10.1021/bi051000k.

[14] A. Boussac, M. Sugiura, F. Rappaport, Probing the quinone binding site of photosystem II from *Thermosynechococcus elongatus* containing either PsbA1 or PsbA3 as the D1 protein through the binding characteristics of herbicides, Biochim. Biophys. Acta 1807 (2010) 119–129, https://doi.org/10.1016/j.bbabio.2010.10.004.

[15] S. de Causmaecker, J.S. Douglass, A. Fantuzzi, W. Nitschke, A.W. Rutherford, Energetics of the exchangeable quinone, Q_B, in photosystem II, Proc. Natl. Acad. Sci. U. S. A. 116 (2019) 19458–19463, https://doi.org/10.1073/pnas.1910675116.

[16] P. Joliot, Period-four oscillations of the flash-induced oxygen formation in photosynthesis, Photosynth. Res. 76 (2003) 65–72, https://doi-org.insb.bib.cnrs.fr/10.1023/A:1024946610564.

[17] B. Kok, B. Forbush, M. McGloin, Cooperation of charges in photosynthetic O_2 evolution–I. A linear four step mechanism, Photochem. Photobiol. 11 (1970) 457–475, https://doi.org/10.1111/j.1751-1097.1970.tb06017.x.

[18] D. Shevela, J.F. Kern, G. Govindjee, J. Messinger, Solar energy conversion by photosystem II: principles and structures, Photosynth. Res. 156 (2023) 279–307, https://doi.org/10.1007/s11120-022-00991-y.

[19] W. Lubitz, D.A. Pantazis, N. Cox, Water oxidation in oxygenic photosynthesis studied by magnetic resonance techniques, FEBS Lett. 597 (2023) 6–29, https://doi.org/10.1002/1873-3468.14543.

[20] G. Renger, Mechanism of light induced water splitting in photosystem II of oxygen evolving photosynthetic organisms, Biochim. Biophys. Acta 1817 (2012) 164–1176, https://doi.org/10.1016/j.bbabio.2012.02.005.

[21] K. Brettel, E. Schlodder, H.T. Witt, Nanosecond reduction kinetics of photooxidized chlorophyll-a (P-680) in single flashes as a probe for the electron pathway, H^+ release and charge accumulation in the O_2-evolving complex, Biochim. Biophys. Acta 766 (1984) 403–415, https://doi.org/10.1016/0005-2728(84)90256-1.

[22] S. Gerken, K. Brettel, E. Schlodder, H.T. Witt, Direct observation of the immediate electron-donor to chlorophyll-a^+ ($P\text{-}680^+$) in oxygen-evolving photosystem-complexes – resolution of manosecond kinetics in the UV, FEBS Lett. 223 (1987) 376–380, https://doi.org/10.1016/0014-5793(87)80322-8.

[23] A.M.A. Hays, I.R. Vassiliev, J.H. Golbeck, R.J. Debus, Role of D1-His190 in the proton-coupled oxidation of tyrosine Y-Z in manganese-depleted photosystem II, Biochemistry 38 (1999) 11851–11865, https://doi.org/10.1021/bi990716a.

[24] D.J. Nürnberg, J. Morton, S. Santabarbara, A. Telfer, P. Joliot, L.A. Antonaru, A. H. Ruban, T. Cardona, E. Krausz, A. Boussac, A. Fantuzzi, A.W. Rutherford, Photochemistry beyond the red-limit in the chlorophyll f-containing photosystems, Science 360 (2018) 1210–1213, https://doi.org/10.1126/science.aar8313.

[25] A.W. Rutherford, A. Osyczka, F. Rappaport, Back-reactions, short-circuits, leaks and other energy wasteful reactions in biological electron transfer: redox tuning to survive life in O_2, FEBS Lett. 586 (2012) 603–616, https://doi.org/10.1016/j.febslet.2011.12.039.

[26] Y. Takegawa, M. Nakamura, S. Nakamura, T. Noguchi, J. Sellés, A.W. Rutherford, A. Boussac, M. Sugiura, New insights on Chl_{D1} function in photosystem II from site-directed mutants of D1/T179 in *Thermosynechococcus elongatus*, Biochim. Biophys. Acta 1860 (2019) 297–309, https://doi.org/10.1016/j.bbabio.2019.01.008.

[27] E. Schlodder, T. Renger, G. Raszewski, W.J. Coleman, P.J. Nixon, R.O. Cohen, B. A. Diner, Site-directed mutations at D1-Thr179 of photosystem II in *Synechocystis* sp. PCC 6803 modify the spectroscopic properties of the accessory chlorophyll in the D1-branch of the reaction center, Biochemistry 47 (2008) 3143–3154, https://doi.org/10.1021/bi702059f.

[28] T. Noguchi, T. Tomo, C. Kato, Triplet formation on a monomeric chlorophyll in the photosystem II reaction center as studied by time-resolved infrared spectroscopy, Biochemistry 40 (2001) 2176–2185, https://doi.org/10.1021/bi0019848.

[29] M. Sugiura, A. Boussac, T. Noguchi, F. Rappaport, Influence of Histidine-198 of the D1 subunit on the properties of the primary electron donor, P680, of photosystem II in *Thermosynechococcus elongatus*, Biochim. Biophys. Acta 1777 (2008) 331–342, https://doi.org/10.1016/j.bbabio.2008.01.007.

[30] M. Sugiura, Y. Inoue, Highly purified thermo-stable oxygen evolving photosystem II core complex from the thermophilic cyanobacterium *Synechococcus elongatus* having His-tagged CP43, Plant Cell Physiol 40 (1999) 1219–1231, https://doi.org/10.1093/oxfordjournals.pcp.a029510.

[31] M. Sugiura, T. Taniguchi, N. Tango, M. Nakamura, J. Sellés, A. Boussac, Probing the role of arginine 323 of the D1 protein in photosystem II function, Physiol. Plant. 171 (2021) 183–199, https://doi.org/10.1111/ppl.13115.

[32] M. Ikeuchi, Y. Inoue, A new 4.8-kDa polypeptide intrinsic to the PS II reaction center, as revealed by modified SDS-PAGE with improved resolution of low-molecular-weight proteins, Plant Cell Physiol. 29 (1988) 1233–1239, https://doi.org/10.1093/oxfordjournals.pcp.a077628.

[33] R. Kale, A.E. Hebert, L.K. Frankel, L. Sallans, T.M. Bricker, P. Pospisil, Amino acid oxidation of the D1 and D2 proteins by oxygen radicals during photoinhibition of photosystem II, Proc. Natl. Acad. Sci. U. S. A. 114 (2017) 2988–2993, https://doi.org/10.1073/pnas.1618922114.

[34] D. Béal, F. Rappaport, P. Joliot, A new high-sensitivity 10-ns time-resolution spectrophotometric technique adapted to in vivo analysis of the photosynthetic apparatus, Rev. Sci. Instrum. 70 (1999) 202–207, https://doi.org/10.1063/1.1149566.

[35] F. Müh, A. Zouni, Extinction coefficients and critical solubilisation concentrations of photosystems I and II from *Thermosynechococcus elongatus*, Biochim. Biophys. Acta 1708 (2005) 219–228, https://doi.org/10.1016/j.bbabio.2005.03.005.

[36] S. Styring, A.W. Rutherford, In the oxygen evolving complex of photosystem II the S_0 state is oxidized to the S_1 state by D^+ (Signal II slow), Biochemistry 26 (1987) 2401–2405, https://doi.org/10.1021/bi00383a001.

[37] J. Lavergne, Improved UV-visible spectra of the S-transitions in the photosynthetic oxygen-evolving system, Biochim. Biophys. Acta 1060 (1991) 175–188, https://doi.org/10.1016/S0005-2728(09)91005-2.

[38] W.F.J. Vermaas, A.W. Rutherford, O. Hansson, Site-directed mutagenesis in photosystem II of the cyanobacterium *Synechocystis* sp. PCC 6803: Donor D is a tyrosine residue in the D2 protein, Proc. Natl. Acad. Sci. USA 85 (1988) 8477–8481, https://doi.org/10.1073/pnas.85.22.8477.

[39] M. Roncel, A. Boussac, J-L. Zurita, H. Bottin, M. Sugiura, D. Kirilovsky, J-M. Ortega, Redox properties of the photosystem II cytochromes b559 and c550 in the cyanobacterium *Thermosynechococcus elongatus*, J. Biol. Inorg. Chem. 8 (2003) 206–216. doi:https://doi.org/10.1007/s00775-002-0406-7.

[40] A. Boussac, J. Sellés, M. Sugiura, What can we still learn from the electrochromic band-shifts in photosystem II? Biochim. Biophys. Acta 2020 (1861) 148176, https://doi.org/10.1016/j.bbabio.2020.148176.

[41] A. Boussac, M. Sugiura, M. Nakamura, R. Nagao, T. Noguchi, S. Viola, A. W. Rutherford, J. Sellés, Photosynth. Res. (2023) in press.

[42] F.J.E. van Mieghem, K. Brettel, B. Hillman, A. Kamlowski, A.W. Rutherford, E. Schlodder, Charge recombination reactions in Photosystem II: 1. Yields, recombination pathways and kinetics of the primary pair, Biochemistry 34 (1995) 4798–4813, https://doi.org/10.1021/bi00014a038.

[43] A.W. Rutherford, A. Krieger-Liszkay, Herbicide-induced oxidative stress in photosystem II, Trends Biochem. Sci. 26 (2001) 648–653, https://doi.org/10.1016/S0968-0004(01)01953-3.

[44] I. Vass, K. Cser, Janus-faced charge recombinations in photosystem II photoinhibition, Trends Plant Sci. 14 (2009) 200–205, https://doi.org/10.1016/j.tplants.2009.01.009.

[45] F.J.E. van Mieghem, W. Nitschke, P. Mathis, A.W. Rutherford, The influence of the quinone-iron electron-acceptor complex on the reaction center photochemistry of photosystem II, Biochim. Biophys. Acta 977 (1989) 207–214, https://doi.org/10.1016/S0005-2728(89)80073-8.

[46] A.W. Rutherford, Orientation of electron-paramagnetic-resonance signals from components in photosystem II membranes, Biochim. Biophys. Acta 807 (1985) 189–201, https://doi.org/10.1016/0005-2728(85)90122-7.

[47] D.L. Kirilovsky, A.G.P. Boussac, F.J.E. van Mieghem, J.-M.R.C. Ducruet, P.R. Setif, J. Yu, W.F.J. Vermaas, A.W. Rutherford, Oxygen-evolving Photosystem II preparation from wild type and Photosystem II mutants of *Synechocystis* Sp. PCC 6803, Biochemistry 31 (1992) 2099–2107, https://doi.org/10.1021/bi00122a030.

[48] A.W. Rutherford, D.R. Paterson, J.E. Mullet, A light-induced spin-polarized triplet detected by EPR in Photosystem II reaction centers, Biochim. Biophys. Acta 635 (1981) 205–214, https://doi.org/10.1016/0005-2728(81)90020-7.

[49] M.C. Thurnauer, J.J. Katz, J.R. Norris, Triplet-state in bacterial photosynthesis – possible mechanisms of primary photo-act, Proc. Natl. Acad. Sci. U. S. A. 72 (1975) 3270–3274, https://doi.org/10.1073/pnas.72.9.3270.

[50] H. Frank, Ö. Hansson, P. Mathis, EPR and optical changes of the photosystem II reaction center produced by low temperature illumination, Photosynth. Res. 20 (1989) 279–289, https://doi.org/10.1007/BF00034070.

[51] G. Raszewski, B.A. Diner, E. Schlodder, T. Renger, Spectroscopic properties of reaction center pigments in photosystem II core complexes: revision of the multimer model, Biophys. J. 95 (2008) 105–119, https://doi.org/10.1529/biophysj.107.123935.

[52] E. Krausz, Selective and differential optical spectroscopies in photosynthesis, Photosynth. Res. 116 (2013) 411–426, https://doi.org/10.1007/s11120-013-9881-7.

[53] N. Cox, J.L. Hughes, R. Steffen, P.J. Smith, A.W. Rutherford, R.J. Pace, E. Krausz, Identification of the Q_Y excitation of the primary electron acceptor of photosystem II: CD determination of its coupling environment, J. Phys. Chem. B 113 (2009) 12364–12374, https://doi.org/10.1021/jp808796x.

[54] M. Judd, J. Morton, D. Nürnberg, A. Fantuzzi, A.W. Rutherford, R. Purchase, N. Cox, E. Krausz, The primary donor of far-red photosystem II: Chl_{D1} or P_{D2}? Biochim. Biophys. Acta 2020 (1861) 148248, https://doi.org/10.1016/j.bbabio.2020.148248.

[55] K. Acharya, B. Neupane, V. Zazubovich, R.T. Sayre, R. Picorel, M. Seibert, R. Jankowiak, Site energies of active and inactive pheophytins in the reaction center of photosystem II from *Chlamydomonas reinhardtii*, J. Phys. Chem. B 116 (2012) 3890–3899, https://doi.org/10.1021/jp3007624.

[56] A.U. Rehman, K. Cser, L. Sass, I. Vass, Characterization of singlet oxygen production and its involvement in photodamage of photosystem II in the cyanobacterium *Synechocystis* PCC 6803 by histidine-mediated chemical trapping, Biochim. Biophys. Acta 1827 (2013) 689–698, https://doi.org/10.1016/j.bbabio.2013.02.016.

[57] Y. Deligiannakis, A.W. Rutherford, Reaction Centre photochemistry in cyanide treated photosystem II, Biochim. Biophys. Acta 1365 (1998) 354–362, https://doi.org/10.1016/S0005-2728(98)00091-7.
[58] A. Klauss, T. Sikora, B. Suss, H. Dau, Fast structural changes (200-900 ns) may prepare the photosynthetic manganese complex for oxidation by the adjacent tyrosine radical, Biochim. Biophys. Acta 1817 (2012) 1196–1207, https://doi.org/10.1016/j.bbabio.2012.04.017.
[59] T. Hayase, Y. Shimada, T. Mitomi, R. Nagao, T. Noguchi, Triplet delocalization over the reaction center chlorophylls in photosystem II 127 (2023) 1758–1770, https://doi.org/10.1021/acs.jpcb.3c00139.
[60] Y. Shibata, S. Nishi, K. Kawakami, J.-R. Shen, T. Renger, Photosystem II does not possess a simple excitation energy funnel: time-resolved fluorescence spectroscopy meets theory, J. Am. Chem. Soc. 135 (2013) 6903–6914, https://doi.org/10.1021/ja312586p.
[61] J. Hanley, Y. Deligiannakis, A. Pascal, P. Faller, A.W. Rutherford, Carotenoid oxidation in photosystem II, Biochemistry 38 (1999) 8189–8195, https://doi.org/10.1021/bi990633u.
[62] P. Faller, C. Fufezan, A.W. Rutherford, In "photosystem II: the light driven water/plastoquinone oxidoreductase", in: T. Wydrzynski, K. Satoh (Eds.), Side-Path Electron Donors in Photosystem II: Cytochrome b559, ChlorophyllZ and β-Carotene, Springer, 2005, pp. 347–365.
[63] L.K. Thompson, G.W. Brudvig, Cytochrome b-559 may function to protect photosystem II from photoinhibition, Biochemistry 27 (1988) 6653–6658, https://doi.org/10.1021/bi00418a002.
[64] A.W. Rutherford, A.R. Crofts, Y. Inoue, Thermo-luminescence as a probe of photosystem II photochemistry – the origin of the flash-induced glow peaks, Biochim. Biophys. Acta 682 (1982) 457–465, https://doi.org/10.1016/0005-2728(82)90061-5.
[65] G.N. Johnson, A. Boussac, A.W. Rutherford, The origin of 40–50°C thermoluminescence bands in photosystem II, Biochim. Biophys. Acta 1184 (1994) 85–92, https://doi.org/10.1016/0005-2728(94)90157-0.
[66] A.W. Rutherford, P. Faller, Photosystem II: evolutionary perspectives, Phil. Trans. R. Soc. Lond. B 358 (2003) 245–253, https://doi.org/10.1098/rstb.2002.1186.
[67] G.A. Davis, A. Kanazawa, M.A. Schöttler, K. Kohzuma, J.E. Froehlich, A. W. Rutherford, M. Satoh-Cruz, D. Minhas, S. Tietz, A. Dhingra, D.M. Kramer, Limitations to photosynthesis by proton motive force-induced photosystem II photodamage, eLife 5 (2016), e16921, https://doi.org/10.7554/eLife.16921.
[68] C.A.R. Cotton, J.S. Douglass, S. De Causmaecker, K. Brinkert, T. Cardona, A. Fantuzzi, A.W. Rutherford, J.M. Murray, Photosynthetic constraints on fuel from microbes, Front. Bioeng. Biotechnol. 3 (2015), https://doi.org/10.3389/fbioe.2015.00036 article 36.
[69] S. Viola, W. Roseby, S. Santabarabara, D. Nürnberg, R. Assunção, H. Dau, J. Sellés, A. Boussac, A. Fantuzzi, A.W. Rutherford, Impact of energy limitations on function and resilience in long-wavelength photosystem II, eLife 11 (2022), e79890, https://doi.org/10.1101/2022.04.05.486971.
[70] S.J. Robles, J. Breton, D.C. Youvan, Partial symmetrization of the photosynthetic reaction center, Science 248 (1990) 1402–1405, https://doi.org/10.1126/science.2192455.
[71] A.K.W. Taguchi, J. Elizabeth Eastman, D.M. Gallo, E. Sheagley, W. Xiao, N. W. Woodbury, Asymmetry requirements in the photosynthetic reaction center of *Rhodobacter capsulatus*, Biochemistry 35 (1996) 3175–3186, https://doi.org/10.1021/bi9521957.
[72] P.D. Laible, C. Kirmaier, C.S.M. Udawatte, S.J. Hofman, D. Holten, D.K. Hanson, Quinone reduction via seconddary B-branch electron transfer in mutant bacterial reaction centers, Biochemistry 42 (2003) 1718–1730, https://doi.org/10.1021/bi026959b.
[73] Z. Perrine, R. Sayre, Modulating the redox potential of the stable electron acceptor, QB, in mutagenized Photosystem II reaction centers, Biochemistry 50 (2011) 1454–1464, https://doi.org/10.1021/bi1017649.
[74] T.J. Beanland, Evolutionary relationships between "Q-type" photosynthetic reaction centres: hypothesis-testing using parsimony, J. Theor. Biol. 145 (1990) 535–545, https://doi.org/10.1016/S0022-5193(05)80487-4.